

SUPPLEMENTARY INFORMATION

Thermal decomposition of hexamethylenetetramine: mechanistic study and identification of reaction intermediates via a computational and NMR approach

Sebastián O. Simonetti,^{a,*} Teodoro S. Kaufman,^a Rodolfo M. Rasia,^b Ariel M. Sarotti,^a Nicolas Grimblat^{a,*}

^aInstituto de Química Rosario (IQUIR, CONICET-UNR), Facultad de Ciencias Bioquímicas y Farmacéuticas - Universidad Nacional de Rosario, Suipacha 531, (2000) Rosario, Argentina; simonetti@iquir-conicet.gov.ar; grimblat@iquir-conicet.gov.ar

^bInstituto de Biología Molecular y Celular de Rosario (IBR, CONICET-UNR), Consejo Nacional de Investigaciones Científicas y Tecnológicas, Universidad Nacional de Rosario, 2000 Rosario, Santa Fe, Argentina

Table of Contents

Description	Page N°
Experimental details	S3
Reagents	S3
Equipment	S3
Chemometrics and graphics software	S3
Synthesis of $^{13}\text{C}^{15}\text{N}$ -hexamethylenetetramine ($^{13}\text{C}_6\text{H}_{12}^{15}\text{N}_4$)	S3
Temperature ramp, 90 min, and 6 hour experiments	S4
NMR spectra acquisition for ^{13}C - ^{15}N -HMTA	S4
Representative NMR spectra	S5
Key signals and crosspeaks observed	S5
Representative spectra at different temperatures and times	S10
Representative NMR spectra of ^{13}C - ^{15}N -HMTA in $\text{AcOH-}d_4$	S12
^1H and ^{13}C NMR of key signals of the main product N-Me in $\text{AcOH-}d_4$ at 363 K	S15
MCR-ALS analysis of the relevant ^1H NMR spectral peaks	S16
Method development and components and variance explained	S16
Decomposition of HMTA. Temperature ramp experiment (303-363 K)	S18
Decomposition of HMTA. 90 min experiment (Temperature = 363 K)	S25
Decomposition of HMTA. 6 hours experiment (Temperature = 363 K)	S32
Kinetic study of the decomposition of HMTA at 363 K	S36
Experimental Procedure	S36
Decomposition rate of HMTA	S37
Decomposition rate of HMTA (initial rate method; up to 20% of decomposition)	S38
Computational methods	S39
General information	S39
Cartesian Coordinates	S40
References	S51

Experimental details

Reagents

The reactions were carried out under an Argon atmosphere, employing oven-dried glassware. Deuterated acetic acid ($\text{AcOH-}d_4$) was purchased from Aldrich Chemical Co. (St. Louis, USA). $^{13}\text{CH}_2\text{O}$ and $^{15}\text{NH}_4\text{Cl}$ were purchased from Santa Cruz Biotechnology (Dallas, USA) and used as received.

Equipment

The ^1H and ^{13}C NMR spectra were acquired with a Bruker Avance 300 spectrometer (Bruker BioSpin GmbH - Rheinstetten, Germany), operating at 300.13 and 75.48 MHz respectively, and a Bruker Avance III 400 MHz spectrometer (400.13 MHz for ^1H , 100.61 MHz for ^{13}C). The resonance of $\text{CH}_3\text{CO}_2\text{H}$ in $\text{AcOH-}d_4$ ($\delta = 2.07$ ppm) was used as an internal standard. The chemical shifts are reported in parts per million in the δ scale and the magnitudes of the coupling constants (J) are given in Hertz. D1 used was 1 s (5 T1), which is the standard to the Bruker NMR apparatus.

The $^{15}\text{N-}^1\text{H}$ HMBC experiments were carried out in a Bruker 700 MHz NMR spectrometer equipped with an Avance III console and a TXI probe (700.2 MHz for ^1H , 176.07 MHz for ^{13}C and 70.95 MHz for ^{15}N).

Chemometrics and graphics software

The NMR spectra were acquired and analyzed with the Topspin v.4.0.6 (Bruker) software. Spectra were exported in ASCII format, for editing and chemometric analysis. The computer routines involving spectral data manipulation were run in Matlab R2015a (Mathworks, Natick, USA). The chemometric analyses were performed with the aid of the MCR-ALS GUI 2.0 (available at <https://mcrals.wordpress.com/download/>) executed in the Matlab environment. Data analyses and graphics were performed employing MCR-ALS results in .txt format, using Origin 8.5 (OriginLab Co., Northampton, USA).

Synthesis of $^{13}\text{C}^{15}\text{N}$ -hexamethylenetetramine ($^{13}\text{C}_6\text{H}_{12}^{15}\text{N}_4$)

^{15}N -Ammonia obtained by heating $^{15}\text{NH}_4\text{Cl}$ (258.3 mg, 4.83 mmol) with CaCl_2 was bubbled into a

beaker containing a solution of $^{13}\text{C}_2\text{H}_2\text{O}$ (750 μL of a solution of 20% wt. in water, 4.83 mmol). The temperature of the solution was kept below 20°C with an ice-bath. When the bubbling stopped, the solution was maintained for 20 min at this temperature. Then, the beaker was heated on a hot plate, removing the water until constant weight. With this procedure, 84.6 mg (0.60 mmol, 75%) of $^{13}\text{C}^{15}\text{N}$ -hexamethylenetetramine was obtained, as a white solid. ^1H NMR ($\text{AcOH-}d_4$): $\delta = 4.92$ ppm (s); ^{13}C NMR: $\delta = 71.6$ ppm; ^{15}N NMR: $\delta = 39.5$ ppm.

Temperature ramp, 90 min and 6 h experiments

Temperature ramp experiment: In an NMR tube, HMTA (50 mg, 0.357 mmol) were dissolved in $\text{AcOH-}d_4$ (0.5 mL). The tube was introduced in the NMR apparatus and ^1H NMR spectra were acquired every 10 K from 298 K to 363 K (8 spectra) in a ramp of 5 K/min. When signal changes were evident, $^1\text{H-}^{13}\text{C}$ -HSQC, $^1\text{H-}^{13}\text{C}$ -HMBC, $^1\text{H-}^1\text{H}$ -COSY, and NOESY spectra were acquired.

90 Min experiment: Once at 363 K, ^1H NMR spectra were acquired every 3 minutes for 90 min. At the end, 2D NMR spectra were acquired, and the probe was left to cool to room temperature. At this point, additional ^1H NMR, ^{13}C NMR, and 2D spectra were acquired.

6 Hours experiment: HMTA (50 mg, 0.357 mmol) was transferred to a Hach tube equipped with a magnetic stir bar, and dissolved in $\text{AcOH-}d_4$. The tube was heated to 363 K and aliquots (50 μL) were taken every hour, transferred to NMR tubes and diluted with $\text{AcOH-}d_4$ to a total volume of 0.5 mL. NMR spectra were acquired. The procedure was repeated six times. Additional ^1H NMR, ^{13}C NMR and 2D spectra were acquired for the last sample.

NMR spectra acquisition for $^{13}\text{C-}^{15}\text{N}$ -HMTA

In an NMR tube, $^{13}\text{C-}^{15}\text{N}$ -HMTA (50 mg, 0.357 mmol) was dissolved in $\text{AcOH-}d_4$ (0.5 mL). ^1H NMR, $^1\text{H-}^{13}\text{C}$ -HSQC, and $^1\text{H-}^{15}\text{N}$ -HMBC spectra were acquired at 298 K; then, the temperature was raised to 348 K in 10 K intervals. An ^1H NMR spectrum was acquired for each interval. At 348 K, ^1H NMR, $^1\text{H-}^{13}\text{C}$ -HSQC, and $^1\text{H-}^{15}\text{N}$ -HMBC spectra were also obtained.

Representative NMR spectra

Key signals and crosspeaks observed

Figure S1. ^1H NMR spectrum of **HMTA** at 298 K in $\text{AcOH-}d_4$. Key signal observed: δ 4.97 ppm.

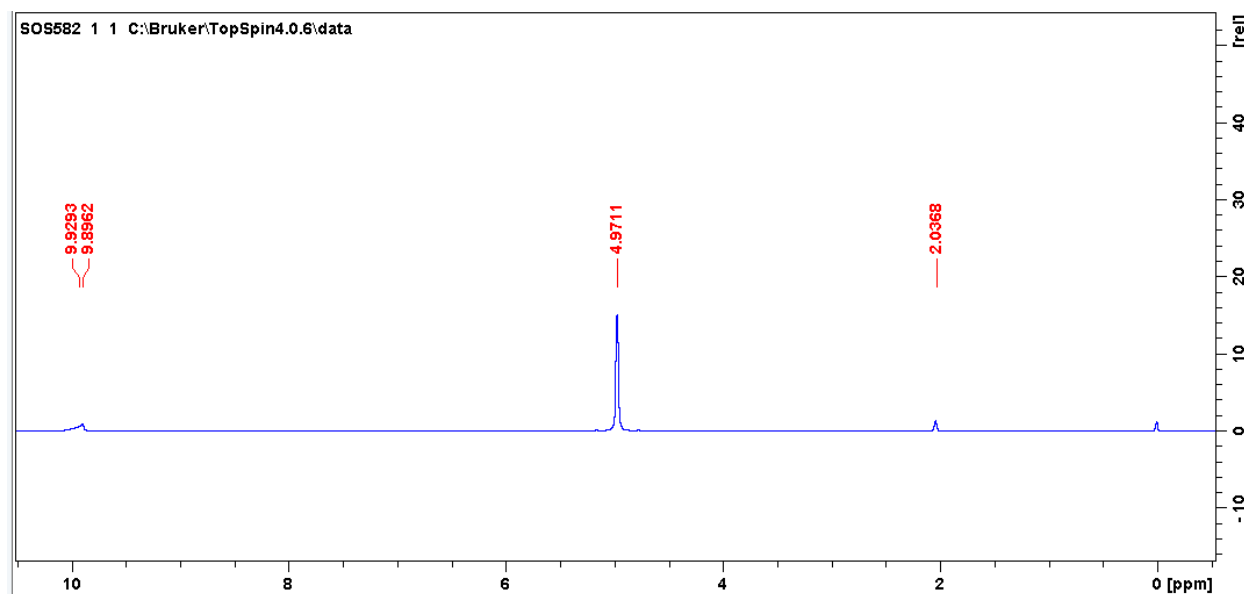


Figure S2. ^1H - ^{13}C -HSQC spectrum of **HMTA** at $T = 298$ K in $\text{AcOH-}d_4$. Key correlation observed: δ 4.97 ppm (^1H) and δ 71.6 ppm (^{13}C).

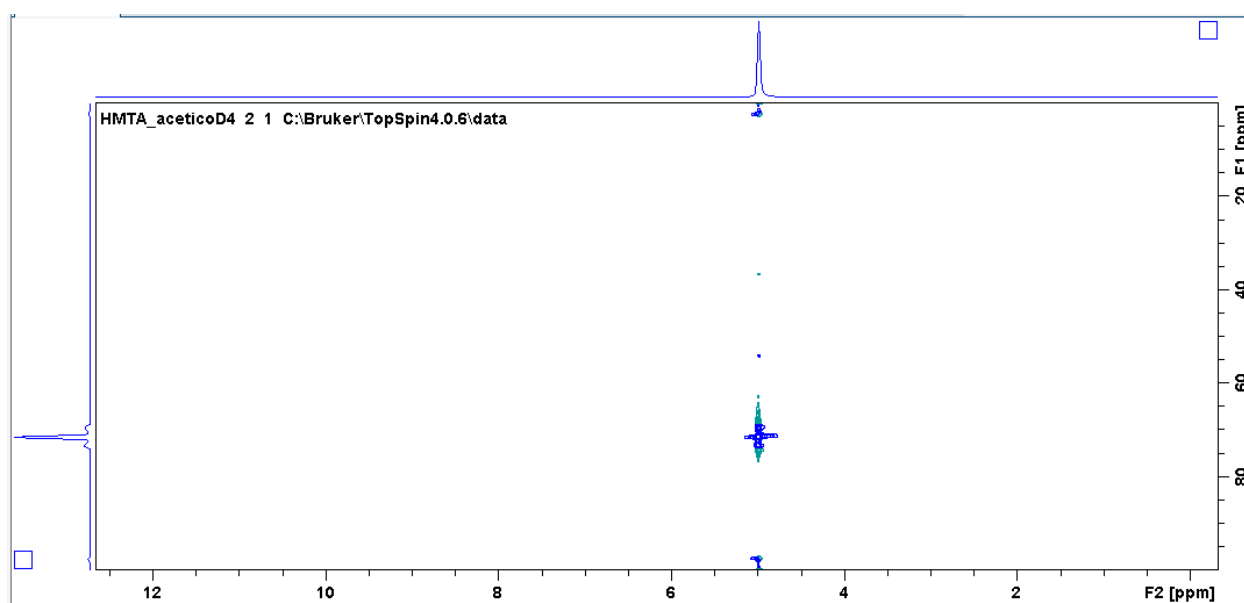


Figure S3. ^1H - ^{15}N -HMBC spectrum of ^{13}C - ^{15}N -HMTA at 298 K in $\text{AcOH-}d_4$. Key correlation observed: δ 4.97 ppm (^1H) and δ 38.7 ppm (^{15}N).

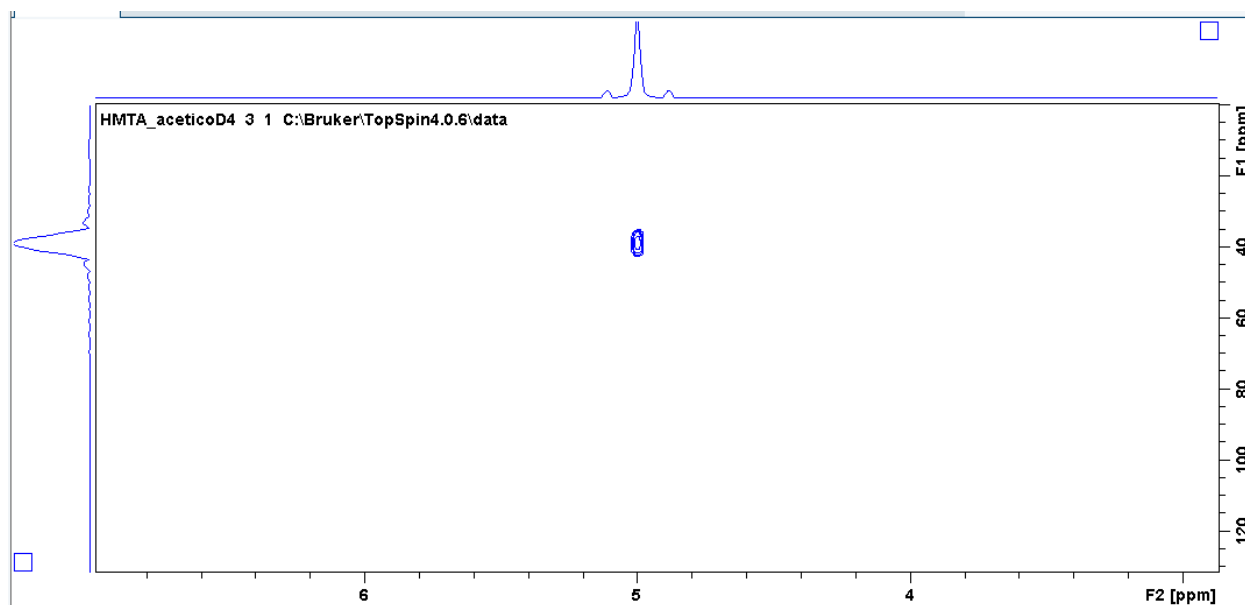


Figure S4. ^1H spectrum of the decomposition of HMTA at 343 K in $\text{AcOH-}d_4$. Key signals observed: δ 4.71 and δ 4.60 ppm (dq), δ 4.97 ppm (s); and δ 5.12 ppm (s).

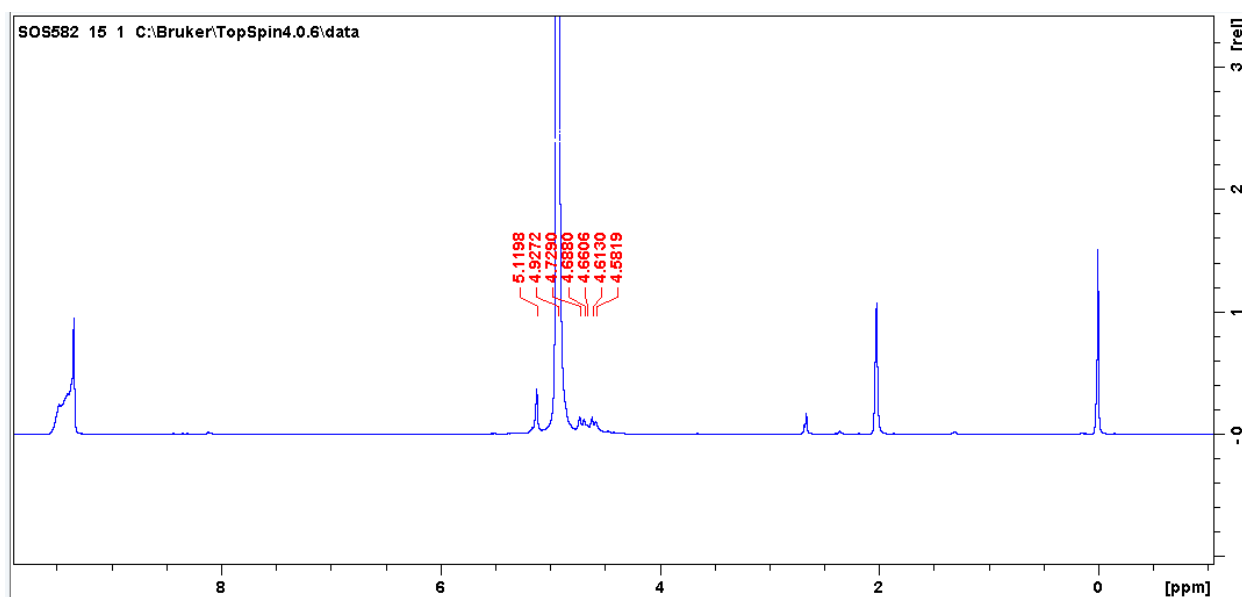


Figure S5. ^1H - ^{13}C -HSQC spectrum of the decomposition of **HMTA** at 343 K in $\text{AcOH-}d_4$. Key correlations observed: δ 4.97 ppm (^1H) with δ 71.6 ppm (^{13}C); δ 4.71 and δ 4.60 ppm (^1H) with δ 70.1 ppm (^{13}C) and δ 5.12 ppm (^1H) with δ 80.7 ppm (^{13}C).

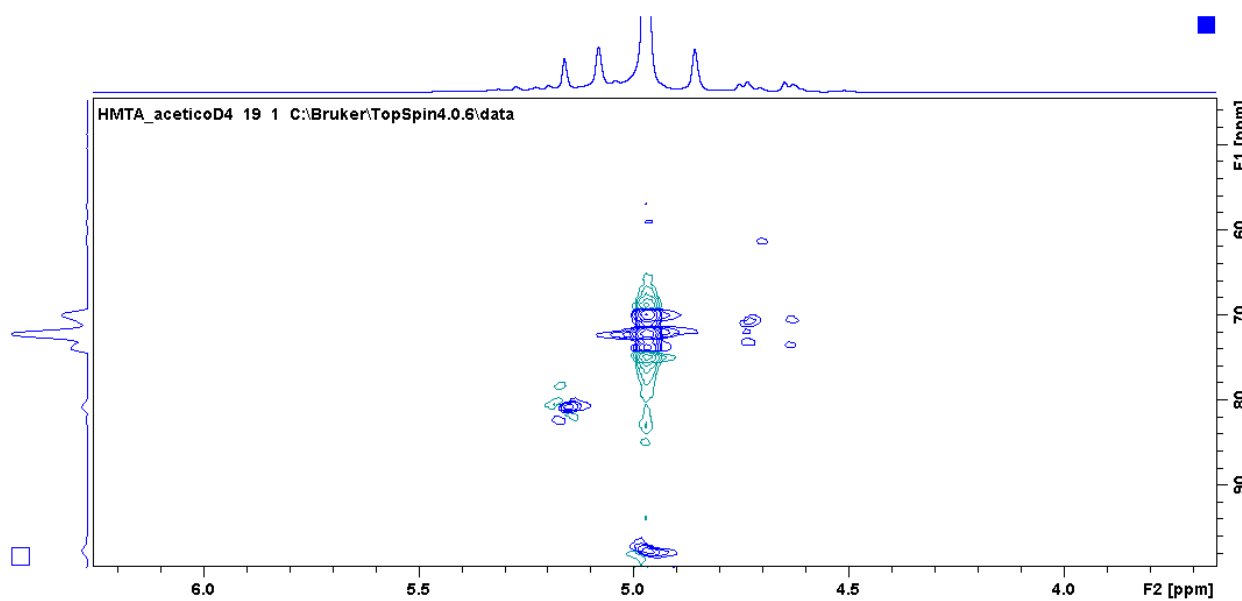


Figure S6. ^1H - ^{15}N -HMBC spectrum of the decomposition of **HMTA** at 343 K in $\text{AcOH-}d_4$. Key correlations observed: δ 4.97 ppm (^1H) with δ 38.97 ppm (^{15}N) and δ 4.71, δ 4.60 and δ 5.12 ppm (^1H) with δ 48.1 ppm (^{15}N).

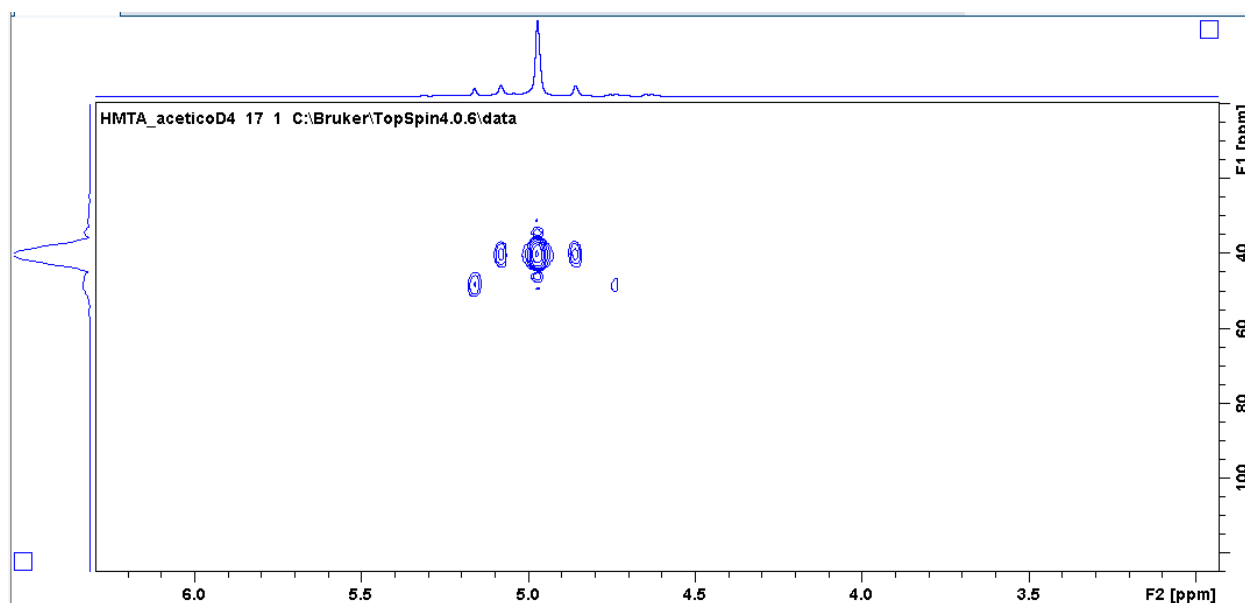


Figure S7. ^1H spectrum of the decomposition of **HMTA** at 353 K in $\text{AcOH-}d_4$. Key signals observed: δ 4.71, δ 4.60 ppm (dd), δ 5.08 ppm (s), δ 5.16 ppm (s), δ 8.14 ppm (d) and δ 8.37 ppm (d).

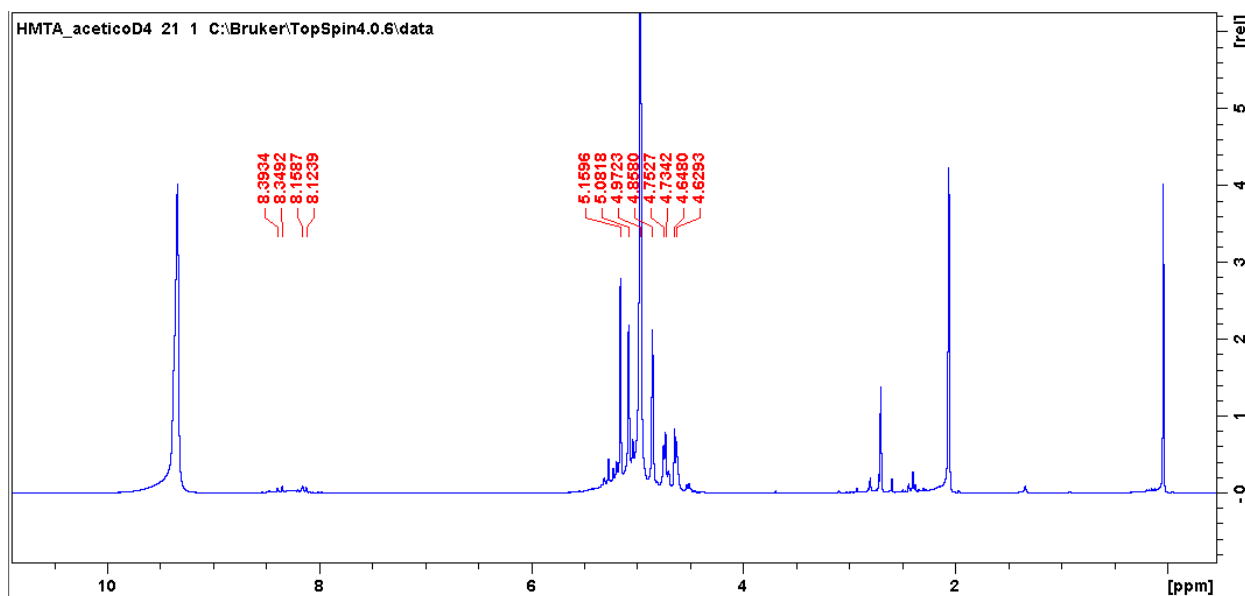


Figure S8. $^1\text{H-}^1\text{H}$ -NOESY spectrum of the decomposition of **HMTA** at 348 K in $\text{AcOH-}d_4$. Inset: Zoom of the region δ 8.00-8.6 ppm. Correlation observed between δ 8.14 ppm (d) and δ 8.37 ppm (d).

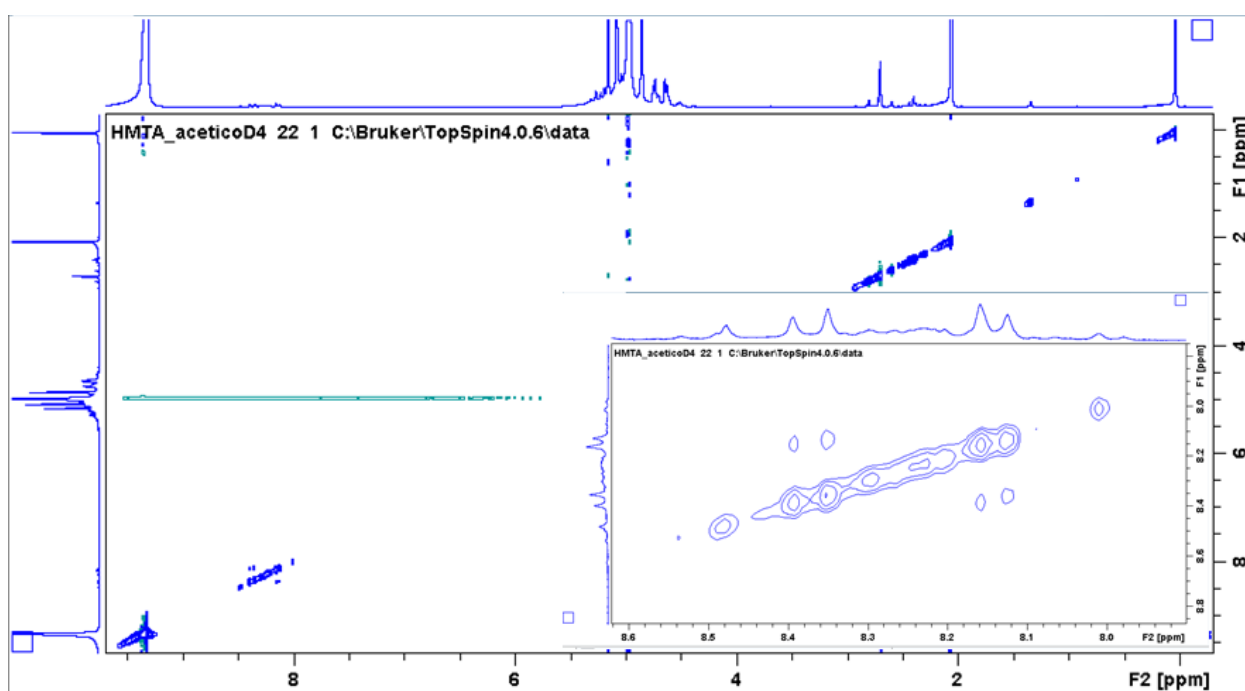


Figure S9. $^1\text{H}^{13}\text{C}$ -HSQC spectrum of the decomposition of **HMTA** at 363 K in $\text{AcOH-}d_4$. Key correlations: δ 2.70 ppm (s, ^1H) with δ 42.6 ppm (^{13}C) and δ 8.16 ppm (s, ^1H) with δ 164.9 ppm (^{13}C).

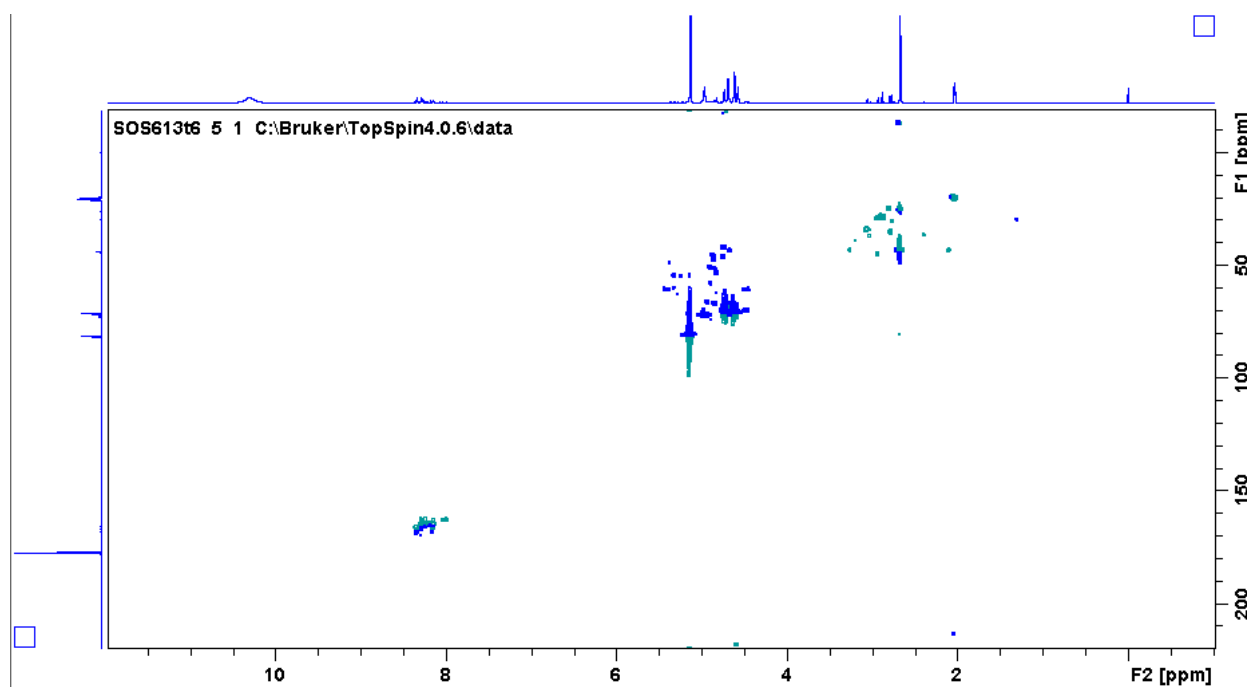
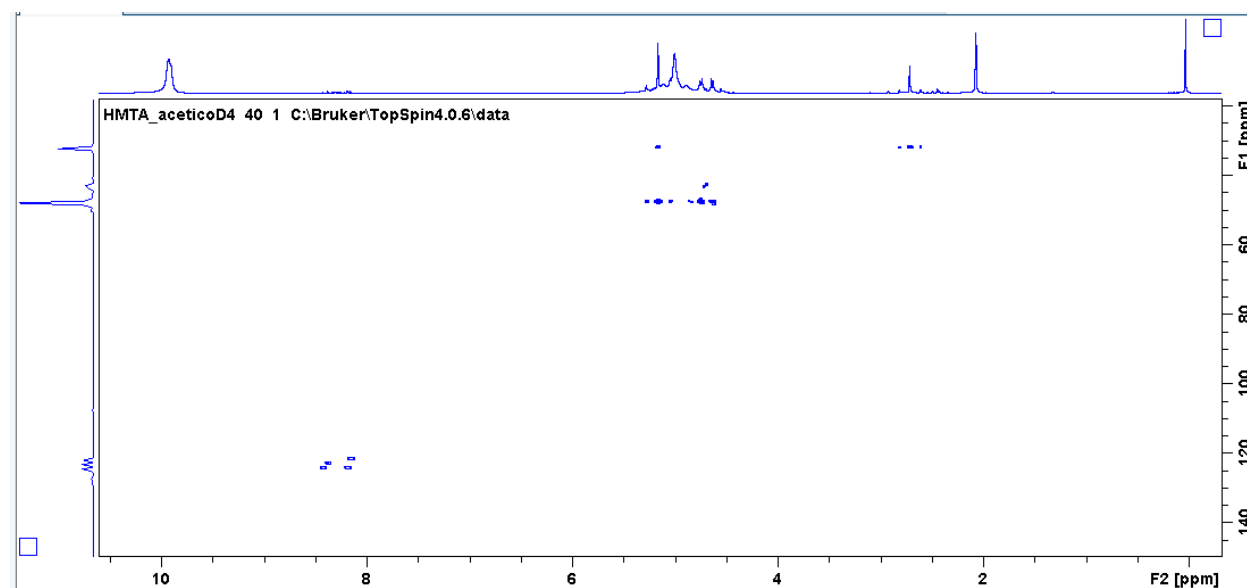


Figure S10. $^1\text{H}^{13}\text{C}$ -HMBC of the decomposition of **HMTA** at 363 K in $\text{AcOH-}d_4$. Key correlations observed: δ 5.12 ppm (^1H) with δ 41.2 ppm (^{13}C).



Representative spectra at different temperatures and times

Figure S11. Decomposition of HMTA in AcOH- d_4 . ^1H NMR spectral comparison at different temperatures. Ramp range: 298-363 K.

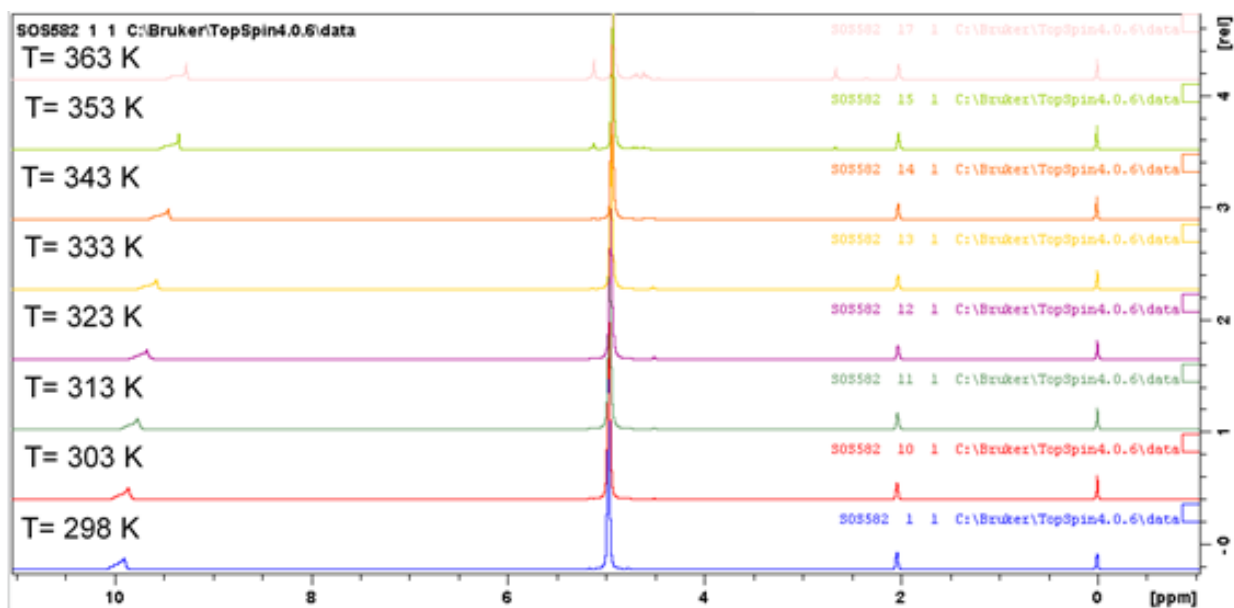


Figure S12. Representative spectra of the ^1H NMR monitoring of the time-dependent evolution of the decomposition of HMTA at 363 K (90 min experiment) in $\text{AcOH-}d_4$.

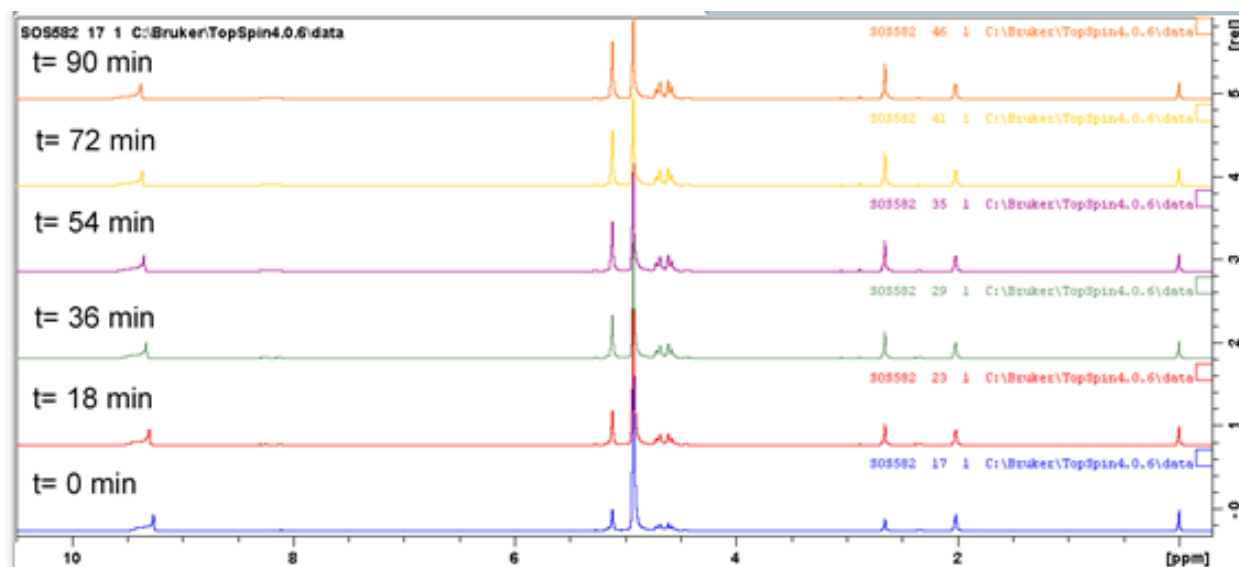
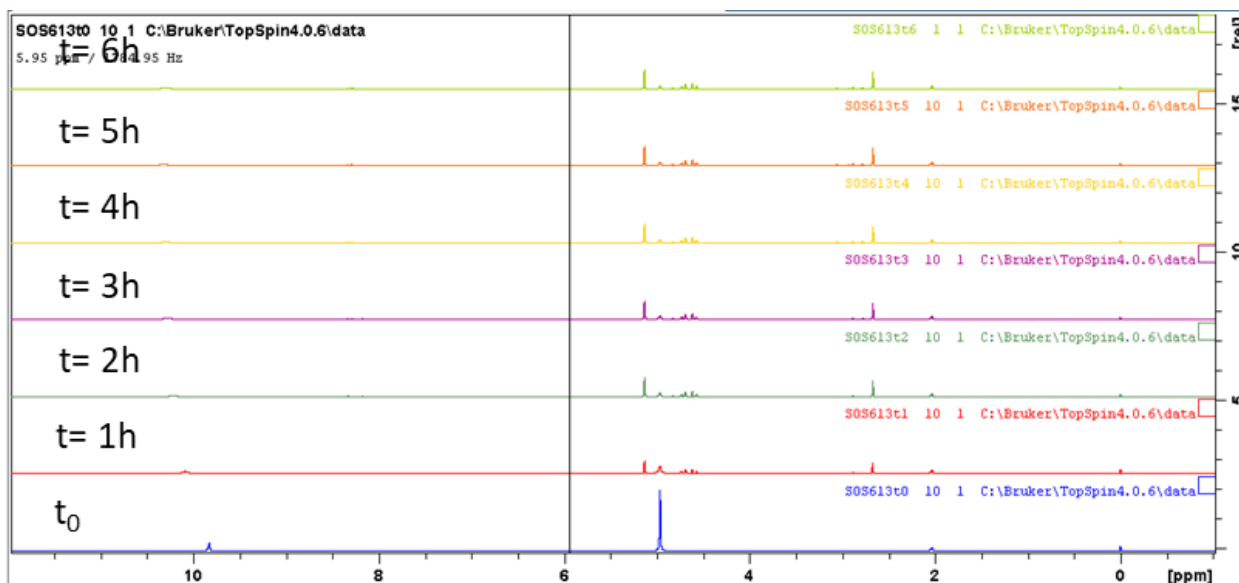


Figure S13. ^1H NMR monitoring of the time-dependent evolution of the decomposition of HMTA at 363 K (6 h experiment) in $\text{AcOH-}d_4$.



Representative NMR spectra of ^{13}C - ^{15}N -HMTA in $\text{AcOH-}d_4$

Figure S14. ^1H - ^{15}N -HMBC spectrum of ^{13}C - ^{15}N -HMTA at 348 K at $t = 0$ min in $\text{AcOH-}d_4$.

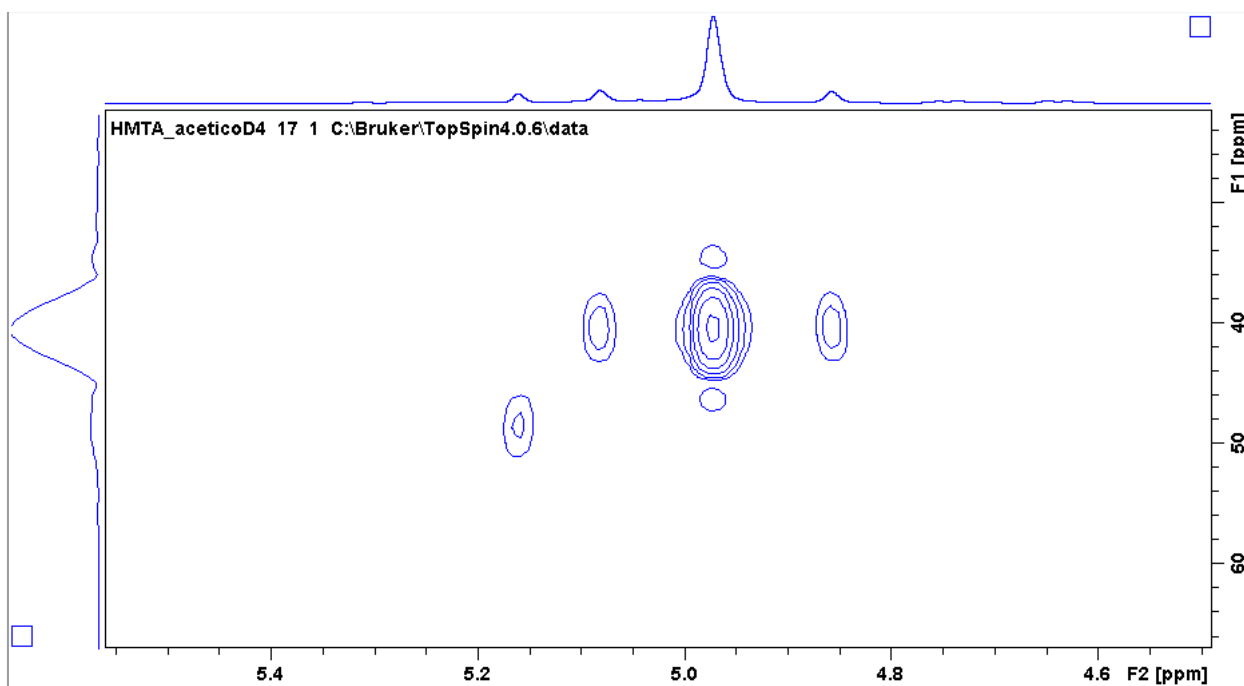


Figure S15. ^1H - ^{15}N -HMBC spectrum of ^{13}C - ^{15}N -HMTA and its decomposition products at 348 K ($t = 30$ min) in $\text{AcOH-}d_4$.

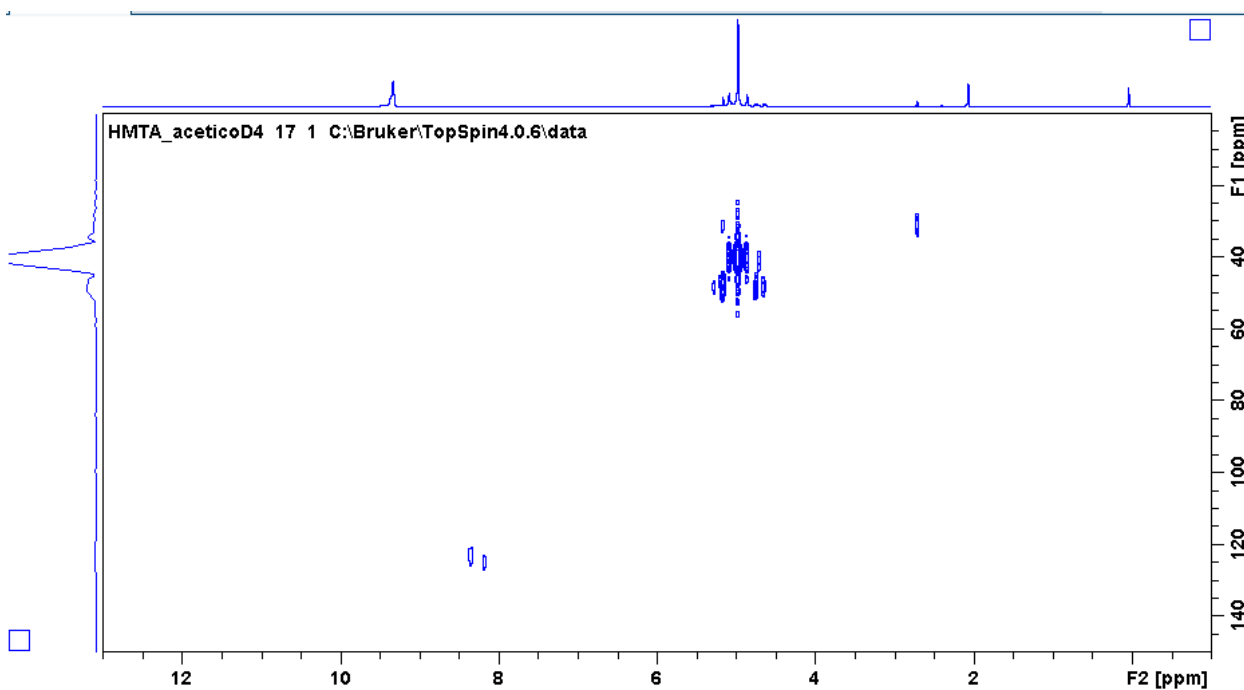


Figure S16. $^1\text{H}^{15}\text{N}$ -HMBC spectrum of ^{13}C - ^{15}N -HMTA and its decomposition products in $\text{AcOH-}d_4$ at 348 K (t = 90 min).

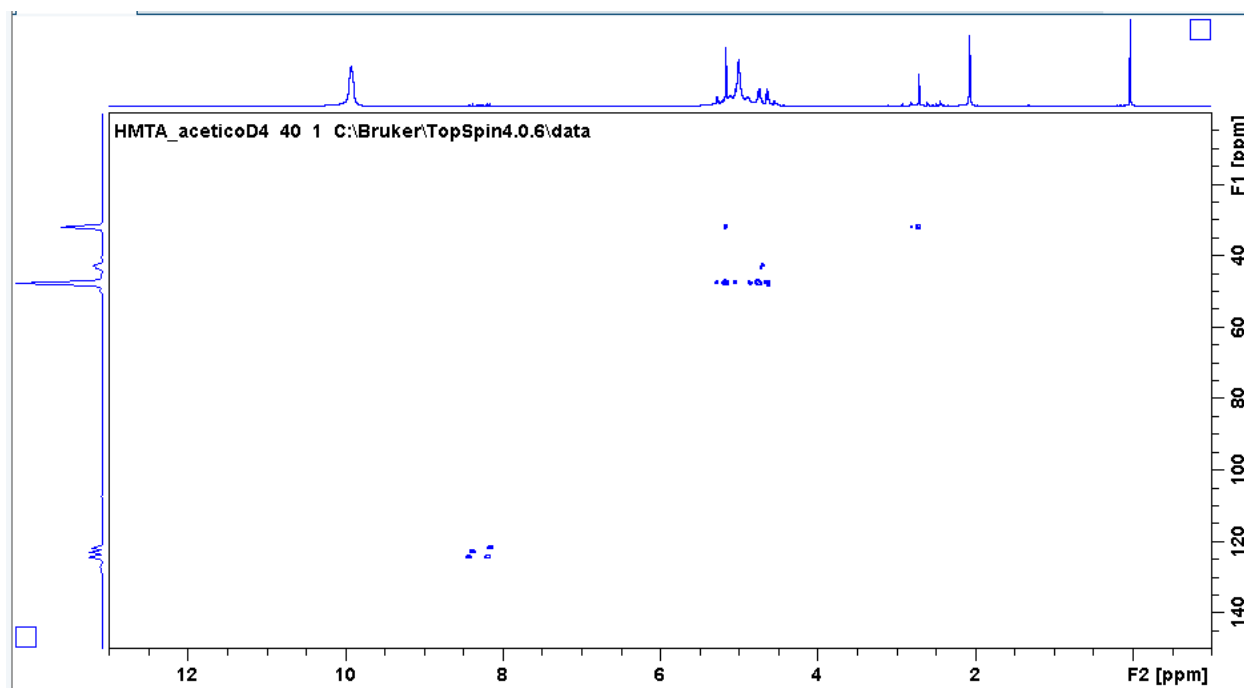


Figure S17. $^1\text{H}^1\text{H}$ -NOESY spectrum of ^{13}C - ^{15}N -HMTA and its decomposition products in $\text{AcOH-}d_4$ at 348 K. Inset: Zoom of the region 8.00-8.6 ppm.

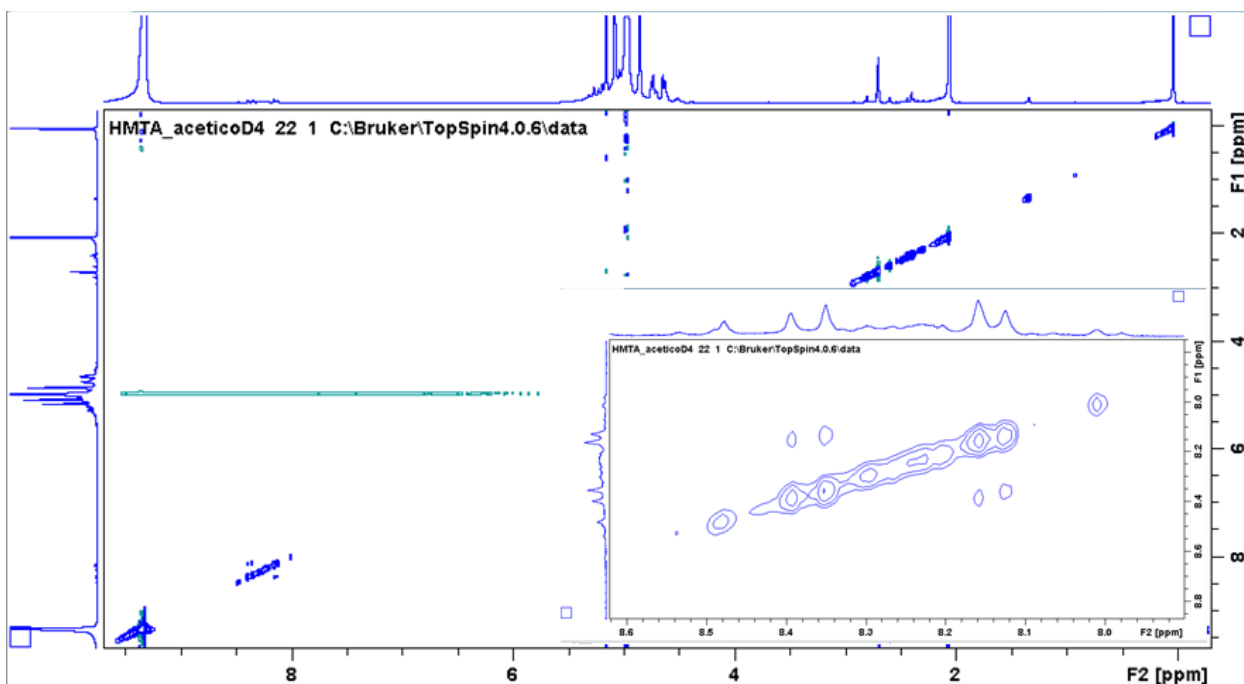
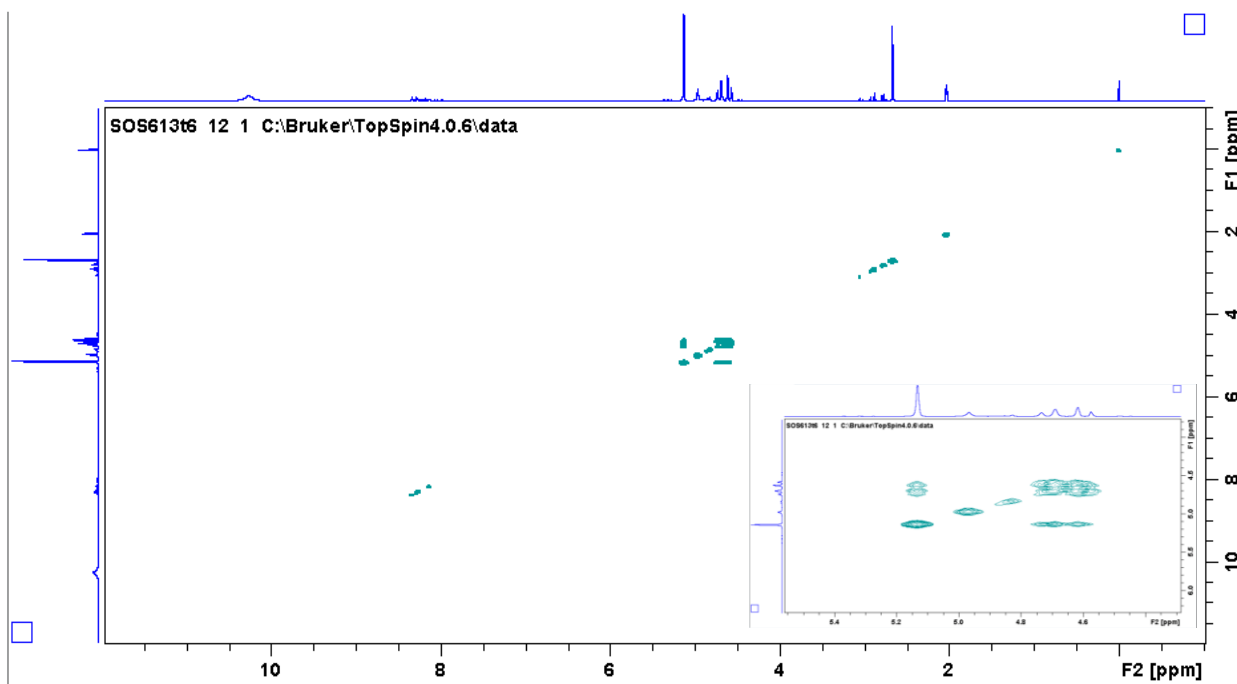


Figure S18. ^1H - ^1H -NOESY spectrum of ^{13}C - ^{15}N -HMTA and its decomposition products in $\text{AcOH-}d_4$ at 348 K. Inset: Zoom of the region 4.50-5.00 ppm.



^1H and ^{13}C NMR of key signals of the main product N-Me in AcOH- d_4 at 363 K

Figure S19. ^1H NMR spectrum of the decomposition of HMTA and detail of key signals.

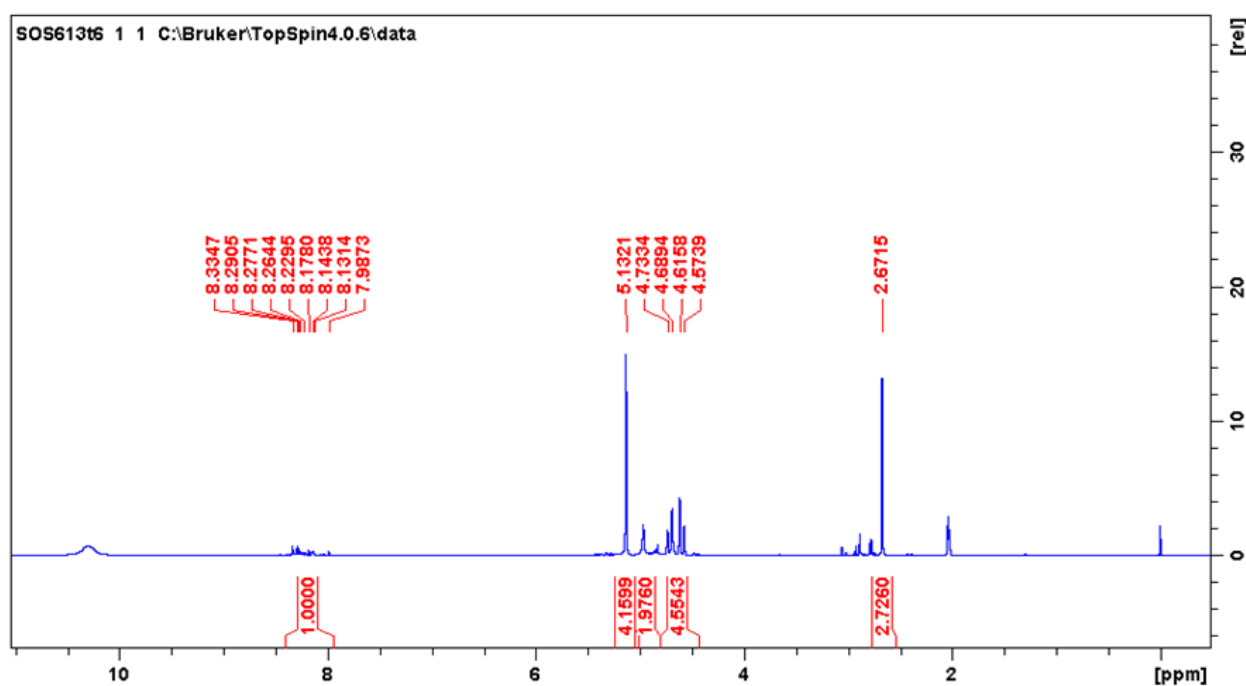
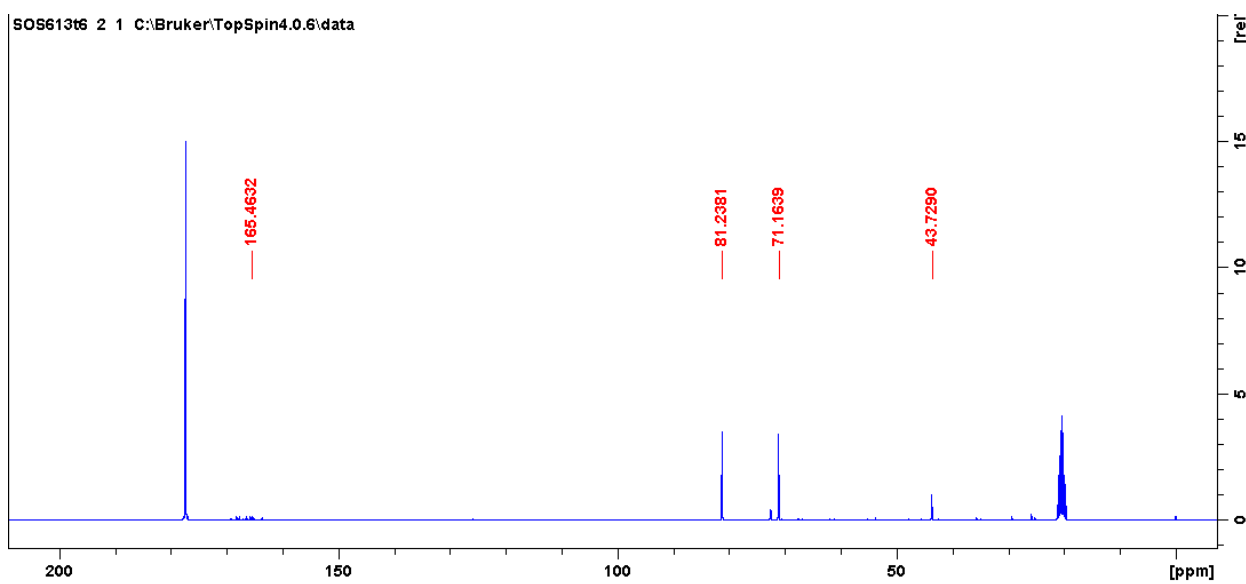


Figure S20. ^{13}C NMR spectrum of the decomposition of HMTA and detail of key signals.



MCR-ALS chemometric analysis of the relevant ^1H NMR spectral peaks

Method development¹

For further processing and analysis, the set of spectra collected during the heating process of each sample was arranged matrix-wise (points \times ppm). Different matrices were prepared by editing the main matrix, removing non-informative regions, and leaving the zones containing the relevant signals. The experiments were subsequently processed by Principal Component Analysis (PCA) in order to determine their chemical rank, i.e., the number of different species responsible for the signal changes observed during the heating process (Table S1).

Then, the Multivariate Curve Resolution algorithm (MCR-ALS) was run in order to obtain the concentration (abundance) profiles of the different species throughout the process, along with the NMR spectra of the corresponding “pure” species involved.² In order to confer physical sense to the results, restrictions such as non-negativity in the concentrations and spectral intensities were applied to the MCR-ALS system. The closure restriction was also added to the concentration values, in order to keep the sum of the relative abundances of the analytes invariable, because the NMR tube was not opened during the experiment. The so obtained “pure” spectra were used to establish the identity of the species involved in the process.

The relative abundance of each signal was calculated using, as reference, the signal of the $\text{CH}_3\text{CO}_2\text{H-}d_4$ ($\delta = 2.00$ ppm; edited matrix between 1.90 and 2.10 ppm), the peak area of which is constant.

Table S1. MCR-ALS analysis of different signals in the ¹H NMR spectra. Number of components and variance explained.

Signal of interest δ (ppm)	Condition (Experiment)	Minimum number of components which explain > 95% variance	Variance Explained (%)
2.57-2.75	Temperature ramp	1	99.29
4.50-4.77	Temperature ramp	3	98.49
4.85-5.00	Temperature ramp	1	97.52
5.09-5.15	Temperature ramp	3	99.97
8.00-8.50	Temperature ramp	2	99.82
2.57-2.75	Time (90 min expt.)	1	99.65
4.50-4.77	Time (90 min expt.)	2	99.93
4.85-5.00	Time (90 min expt.)	1	99.19
5.09-5.15	Time (90 min expt.)	2	99.99
8.00-8.50	Time (90 min expt.)	2	99.99
2.57-2.75	Time (6 h expt.)	1	98.53
4.50-4.77	Time (6 h expt.)	1	99.88
4.85-5.00	Time (6 h expt.)	1	98.41
5.09-5.15	Time (6 h expt.)	1	99.41
8.00-8.50	Time (6 h expt.)	1	98.23

Decomposition of HMTA. Temperatura ramp experiment (303-363 K)

Figure S21. Left: ^1H NMR spectrum of HMTA and its decomposition products in the region $\delta_{\text{H}} = 2.60\text{-}2.80$ ppm. Right: Signal overlap with the “pure” spectrum provided by MCR-ALS analysis.

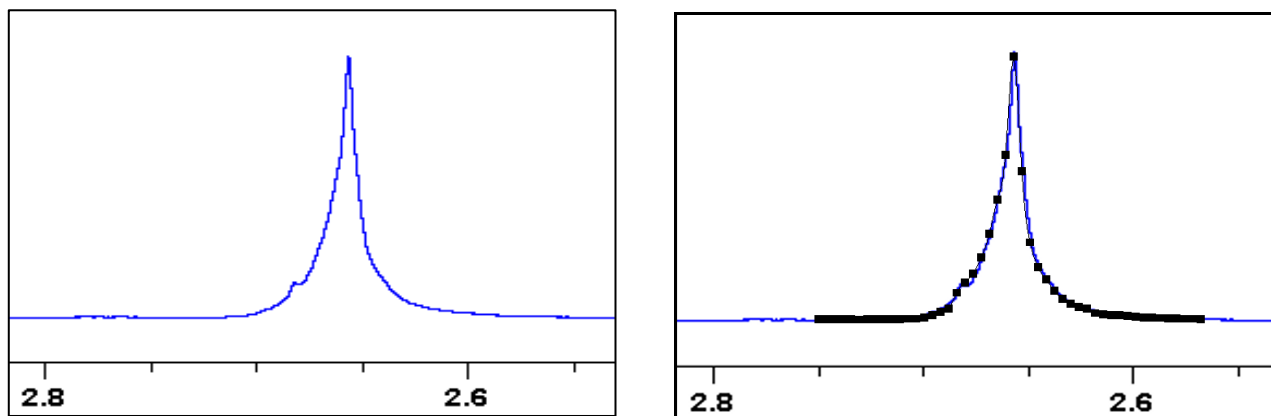


Figure S22. Temperature-dependent evolution of the abundance of **N-Me** according to the MCR-ALS analysis for one component of the ^1H NMR spectra of HMTA and its decomposition products in the region $\delta_{\text{H}} = 2.60\text{-}2.80$ ppm.

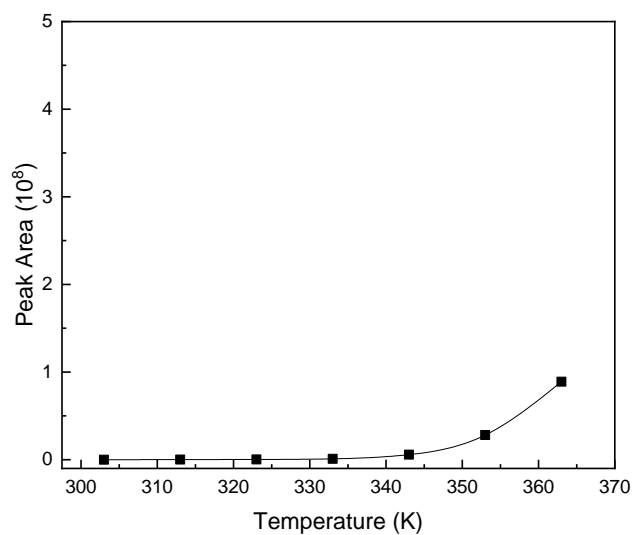


Figure S23. Left: ^1H NMR spectrum of HMTA and its decomposition products in the region $\delta_{\text{H}} = 4.50\text{-}4.77$ ppm. Right: Signal overlap with the “pure” spectrum provided by MCR-ALS analysis.

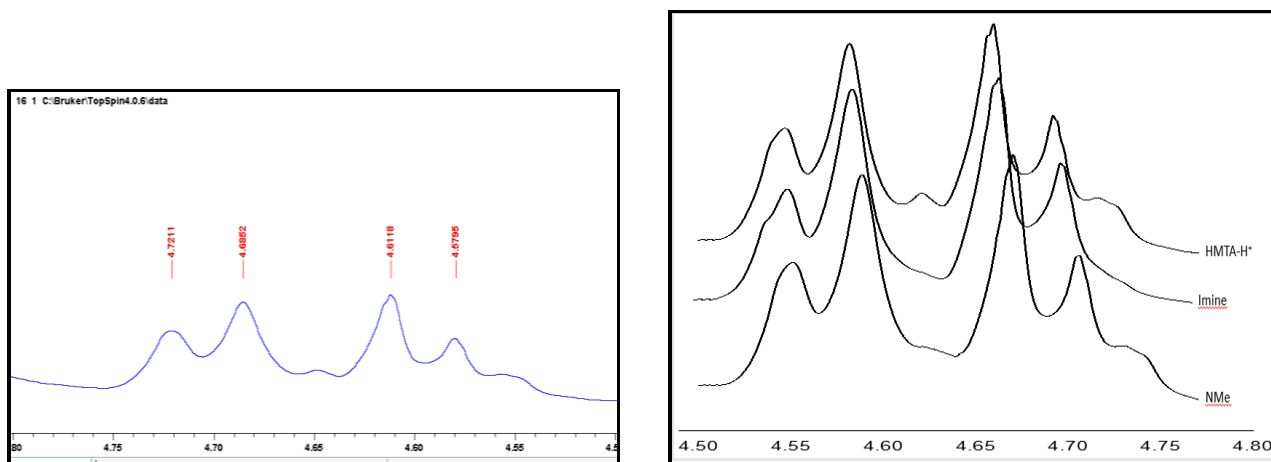


Figure S24. Temperature-dependent evolution of the abundance of **HMTAD⁺** (top), **Iminium** (middle) and **N-Me** (right) according to the MCR-ALS analysis with three components of the ¹H NMR spectrum of HMTA and its decomposition products in the region $\delta_H = 4.50$ - 4.77 ppm.

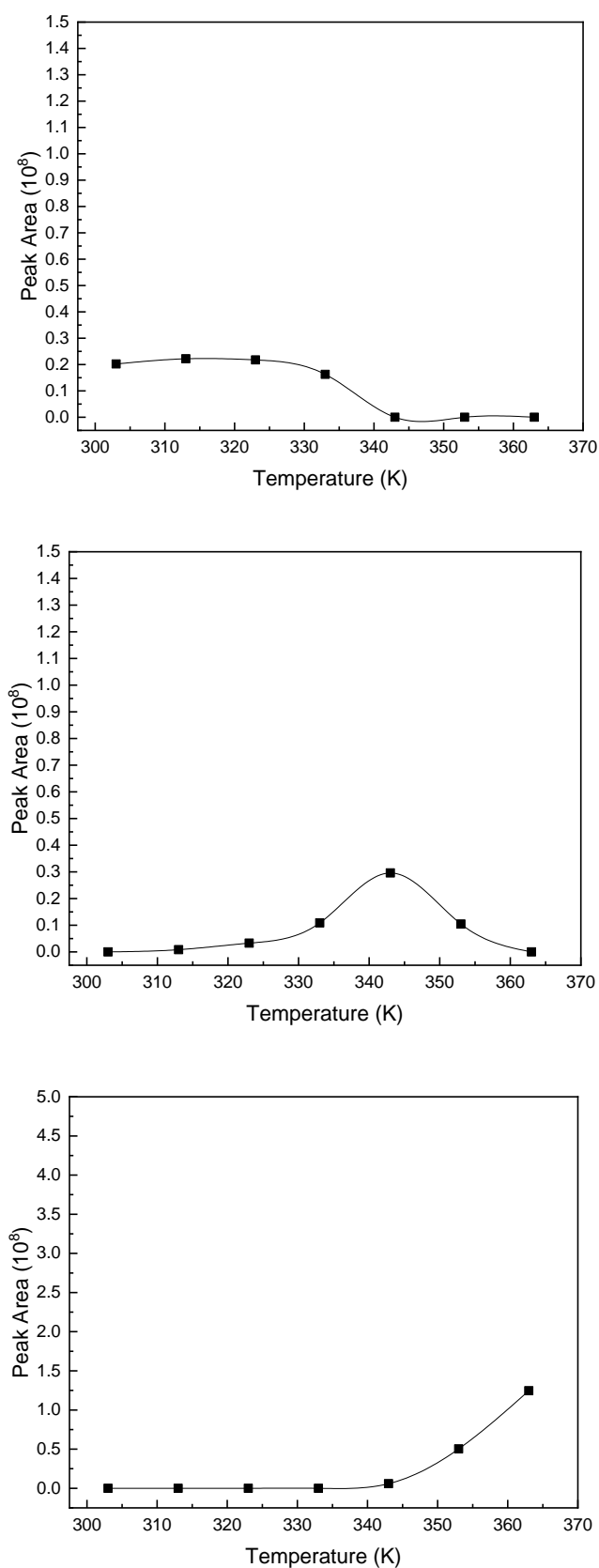


Figure S25. Left: ^1H NMR spectrum of HMTA and its decomposition products in the region $\delta_{\text{H}} = 4.80\text{-}5.00$ ppm. Right: Signal overlap with the “pure” spectrum provided by MCR-ALS analysis.

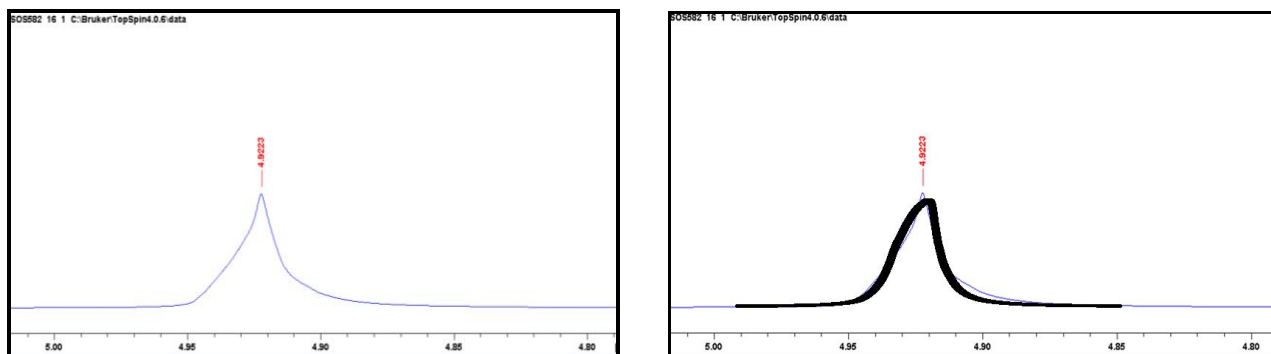


Figure S26. Temperature-dependent evolution of the abundance of **HMTA** according to the MCR-ALS analysis with one component of the ^1H NMR spectrum of HMTA and its decomposition products in the region $\delta_{\text{H}} = 4.80\text{-}5.00$ ppm.

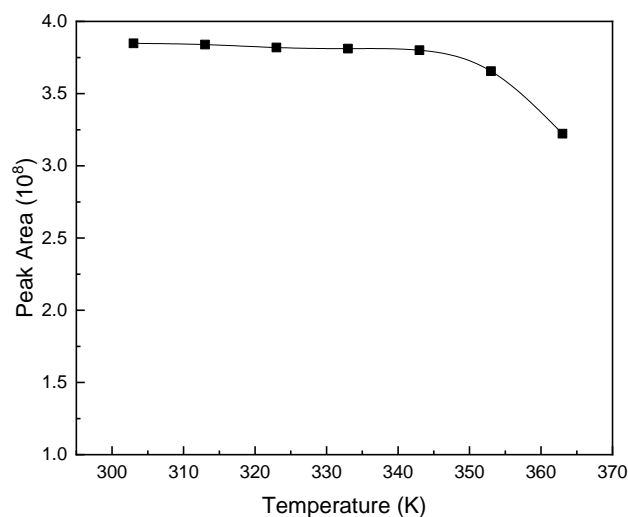


Figure S27. Left: ^1H NMR spectrum of HMTA and its decomposition products in the region $\delta_{\text{H}} = 5.09\text{-}5.14$ ppm. Right: Signal overlap with the “pure” spectrum provided by MCR-ALS analysis.

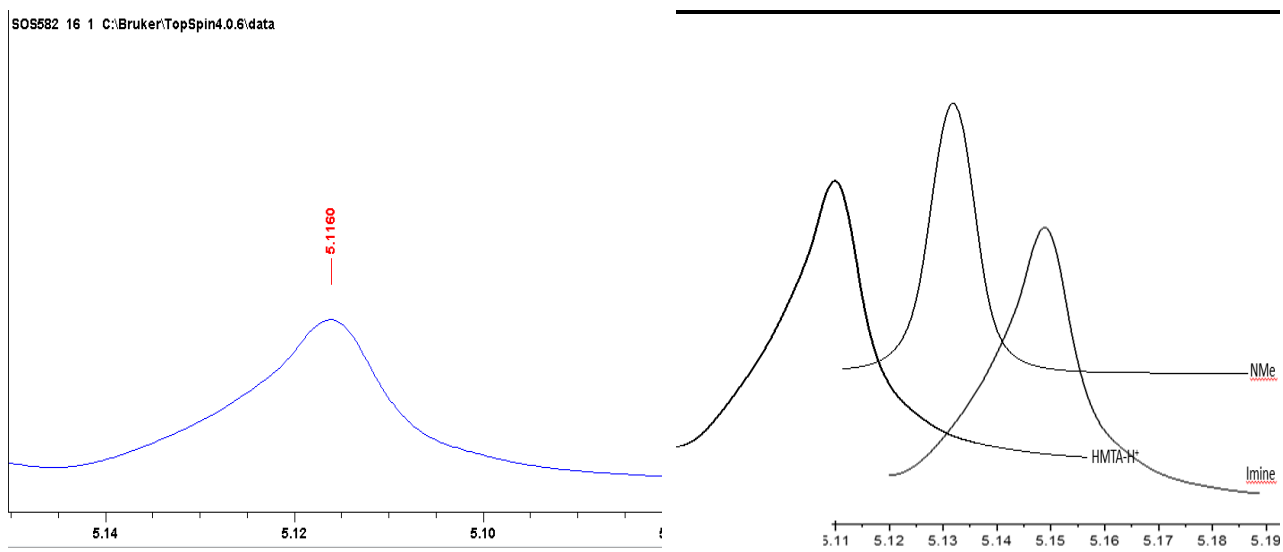
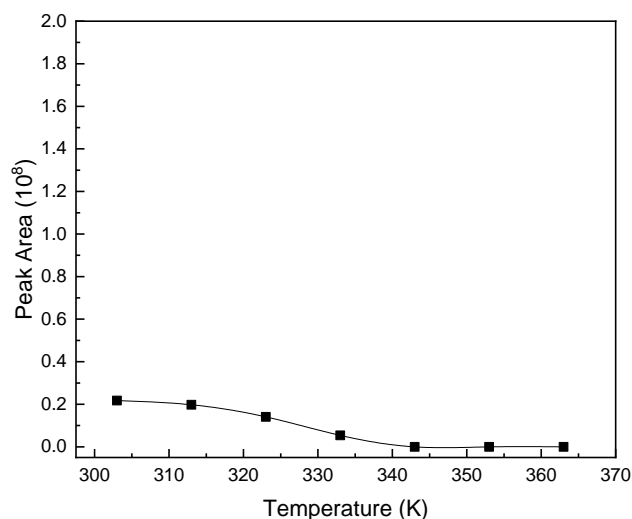


Figure S28. Temperature-dependent evolution of the abundance of **HMTAD⁺** (top) and **Iminium** (middle) and **N-Me** (bottom) according to the MCR-ALS analysis with three components of the ^1H NMR spectrum of HMTA and its decomposition products in the region $\delta_{\text{H}} = 5.10\text{-}5.16$ ppm.



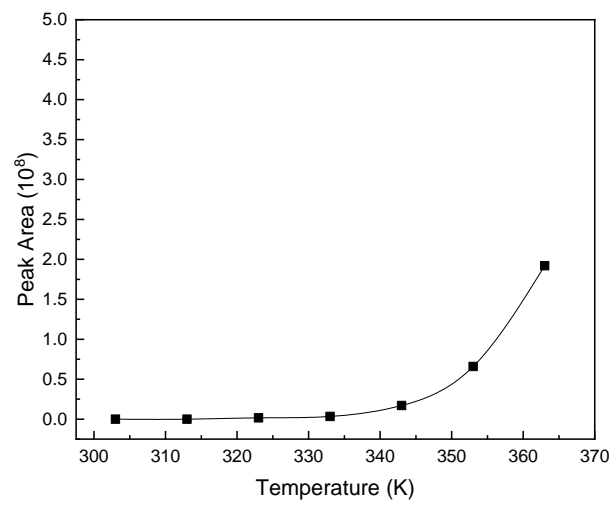
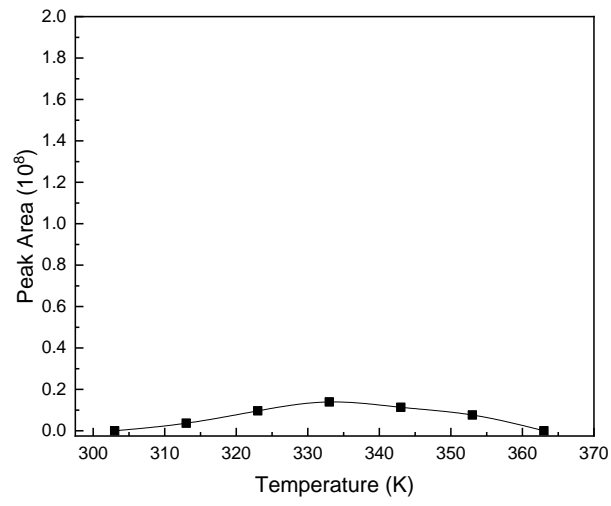


Figure S29. Left: ^1H NMR spectrum of HMTA and its decomposition products in the region $\delta_{\text{H}} = 8.00\text{-}8.50$ ppm. Right: Signal overlap with the “pure” spectrum provided by MCR-ALS analysis.

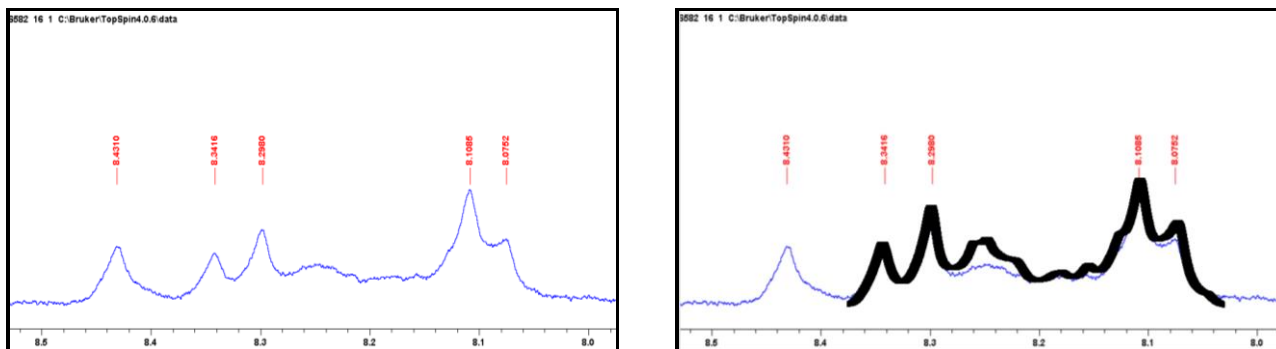
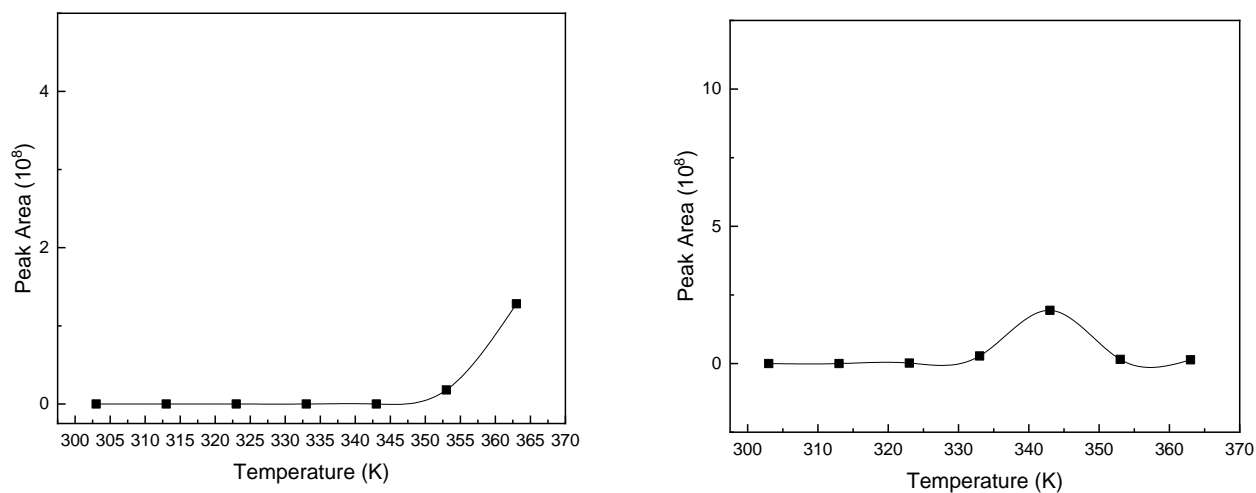


Figure S30. Temperature-dependent evolution of the abundance of **Iminium** (left) and **N-Me** (right) according to the MCR-ALS analysis with two components of the ^1H NMR spectra of HMTA and its decomposition products in the region $\delta_{\text{H}} = 8.00\text{-}8.50$ ppm.



Decomposition of HMTA. 90 min experiment (Temperature = 363 K)

Figure S31. Left: ^1H NMR spectrum of HMTA and its decomposition products in the region $\delta_{\text{H}} = 2.60\text{-}2.80$ ppm, at time = 90 min. Right: Signal overlap with the “pure” spectrum provided by MCR-ALS analysis.

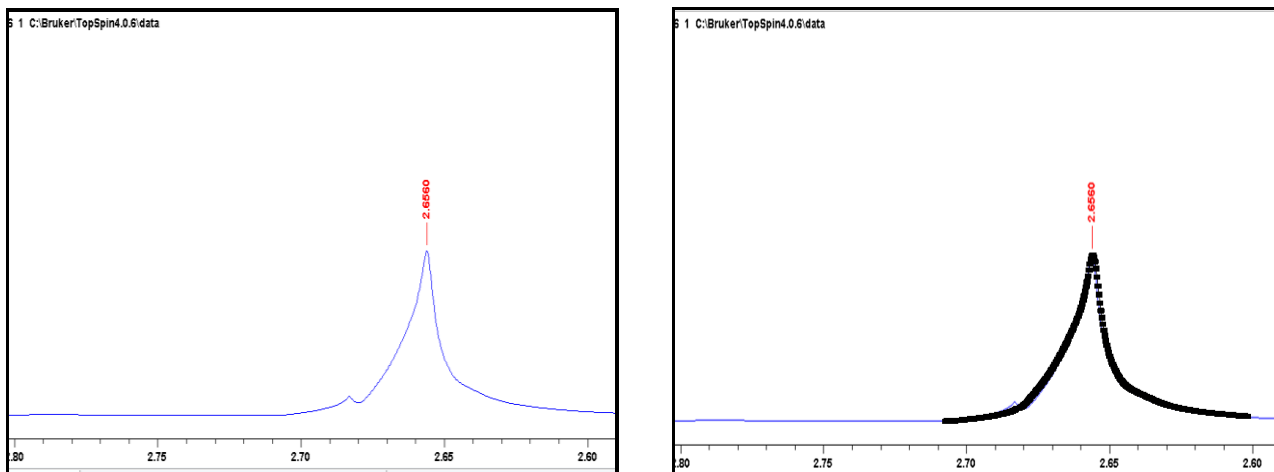


Figure S32. Time-dependent evolution of the abundance of **N-Me** according to the MCR-ALS analysis with one component of the ^1H NMR spectra of HMTA and its decomposition products in the region $\delta_{\text{H}} = 2.60\text{-}2.80$ ppm.

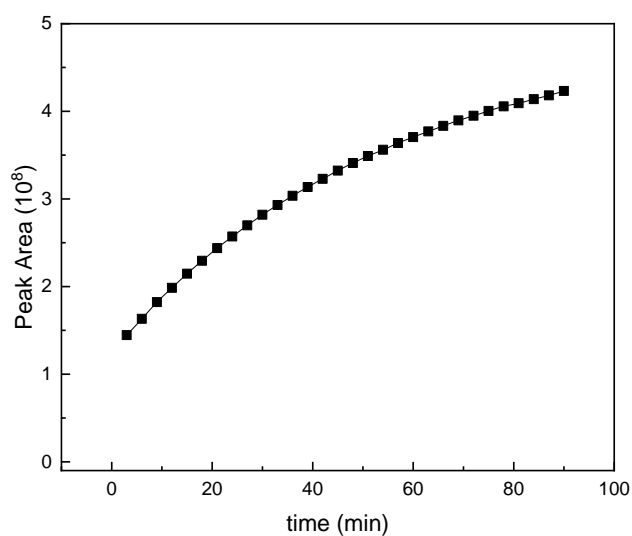


Figure S33. Left: Zoom of the ^1H NMR spectrum of HMTA and its decomposition products in the region $\delta_{\text{H}} = 4.50\text{--}4.77$ ppm, at time = 90 min. Right: Signal overlap with the “Pure” spectra of HMTA- H^+ Imine and NMe provided by MCR-ALS”.

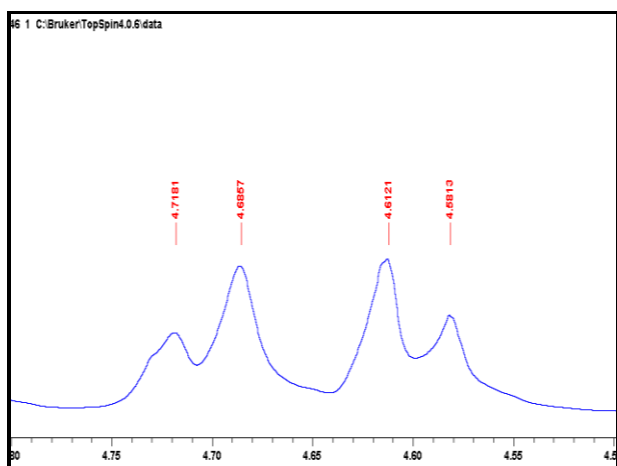


Figure S34. Time-dependent evolution of the abundance of **Iminium** (top) and **N-Me** (bottom) according to the MCR-ALS analysis with two components of the ^1H NMR spectrum of HMTA and its decomposition products in the region $\delta_{\text{H}} = 4.50\text{-}4.77$ ppm.

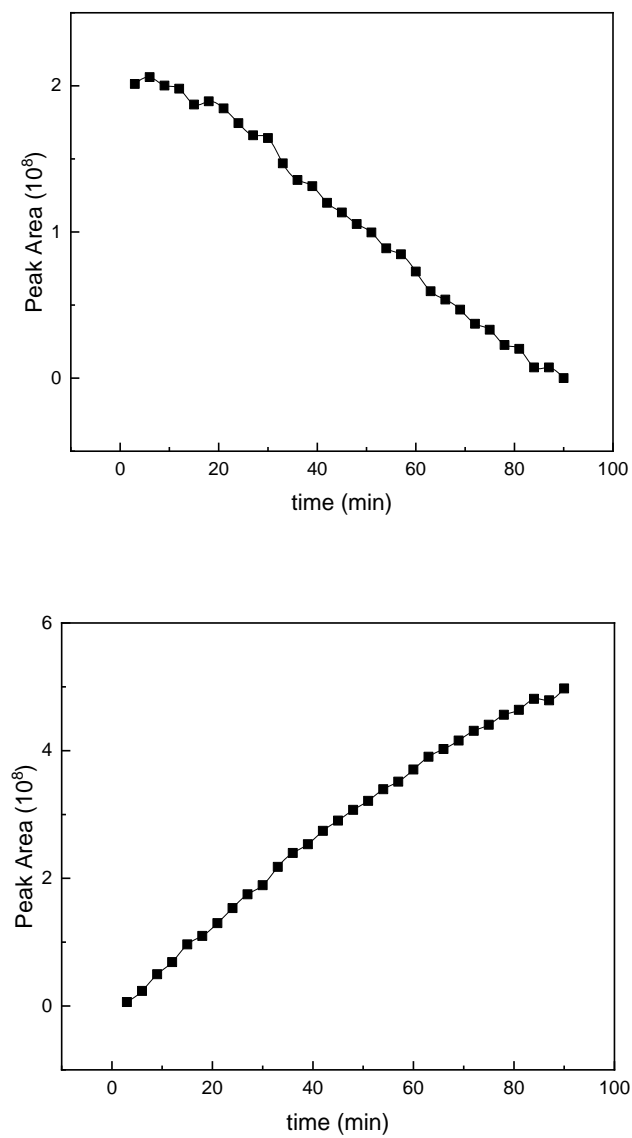


Figure S35. Left: ^1H NMR spectrum of HMTA and its decomposition products in the region $\delta_{\text{H}} = 4.90\text{-}5.00$ ppm, at time = 90 min. Right: Signal overlap with the “Pure” spectrum provided by MCR-ALS.

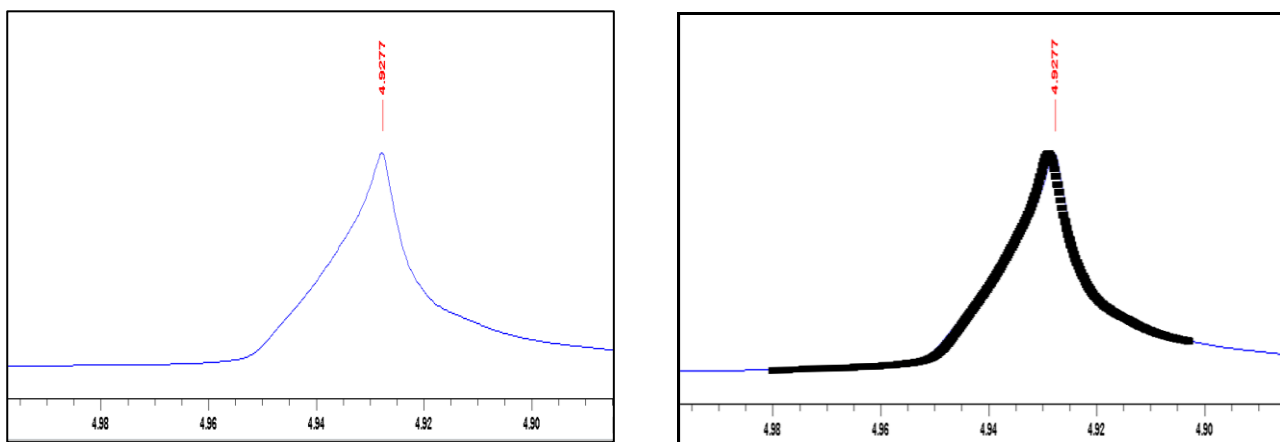


Figure S36. Time-dependent evolution of the abundance of **HMTA** according to the MCR-ALS analysis with one component of the ^1H NMR spectrum of HMTA and its decomposition products in the region $\delta_{\text{H}} = 4.80\text{-}5.00$ ppm.

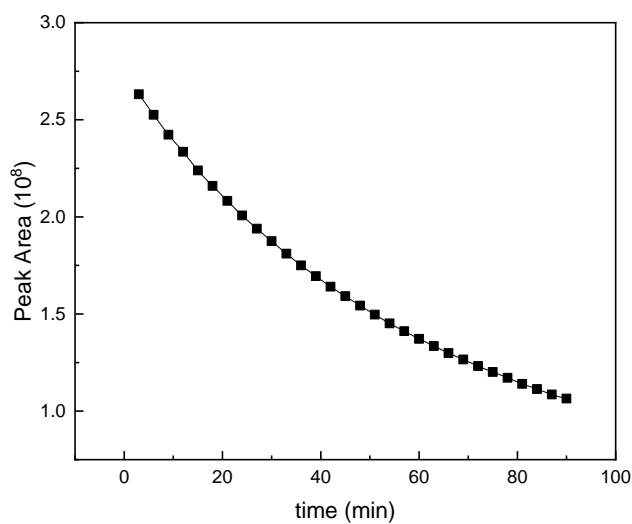


Figure S37. ^1H NMR spectrum of HMTA and its decomposition products in the region $\delta_{\text{H}} = 5.10$ - 5.16 ppm. Right: Signal overlap with the “Pure” spectrum provided by MCR-ALS.

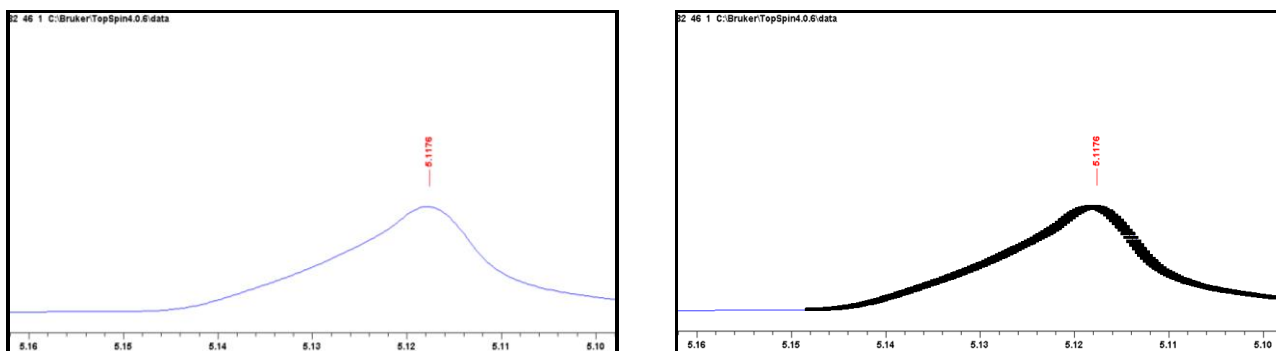


Figure S38. Time-dependent evolution of the abundance of **N-Me** according to the MCR-ALS analysis with one component of the ^1H NMR spectrum of HMTA and its decomposition products in the region $\delta_{\text{H}} = 5.10$ - 5.16 ppm.

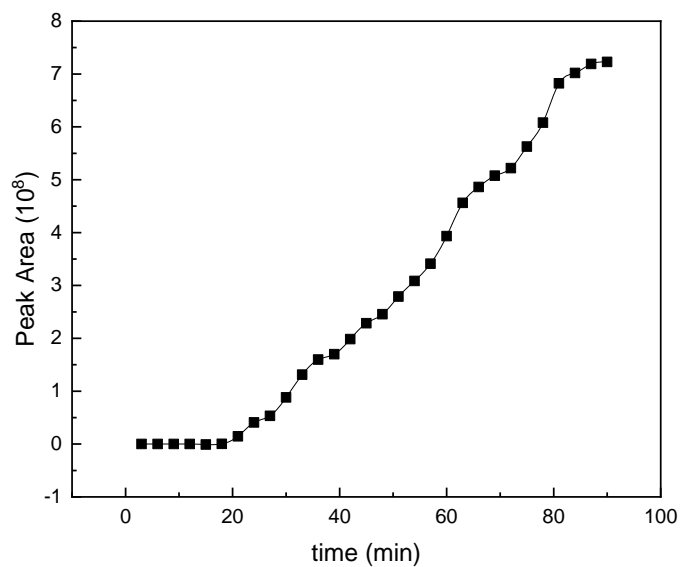
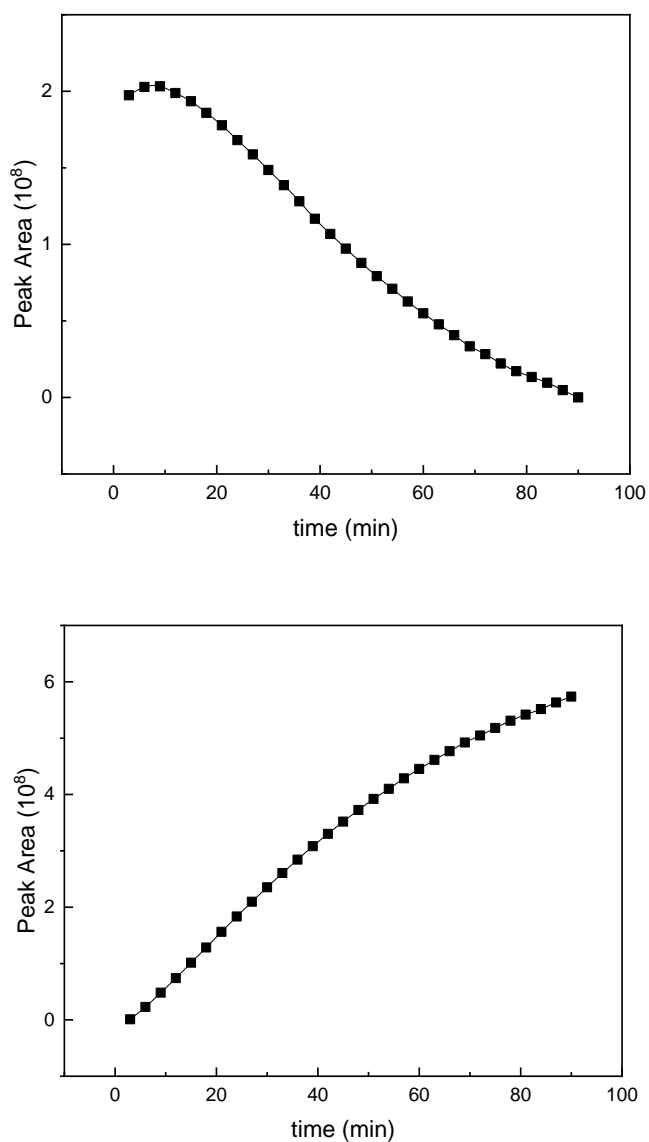


Figure S39. Time-dependent evolution of the abundance of **Iminium** (top) and **N-Me** (bottom) according to the MCR-ALS analysis with two components of the ^1H NMR spectrum of HMTA and its decomposition products in the region $\delta_{\text{H}} = 8.00\text{-}8.50$ ppm.



Decomposition of HMTA. 6 hours experiment (Temperature = 363 K)

Figure S40. Left: ^1H NMR spectrum of HMTA and its decomposition products in the region $\delta_{\text{H}} = 2.60\text{-}2.70$ ppm. Right: Signal overlap with the corresponding “pure” NMR spectrum provided by MCR-ALS analysis.

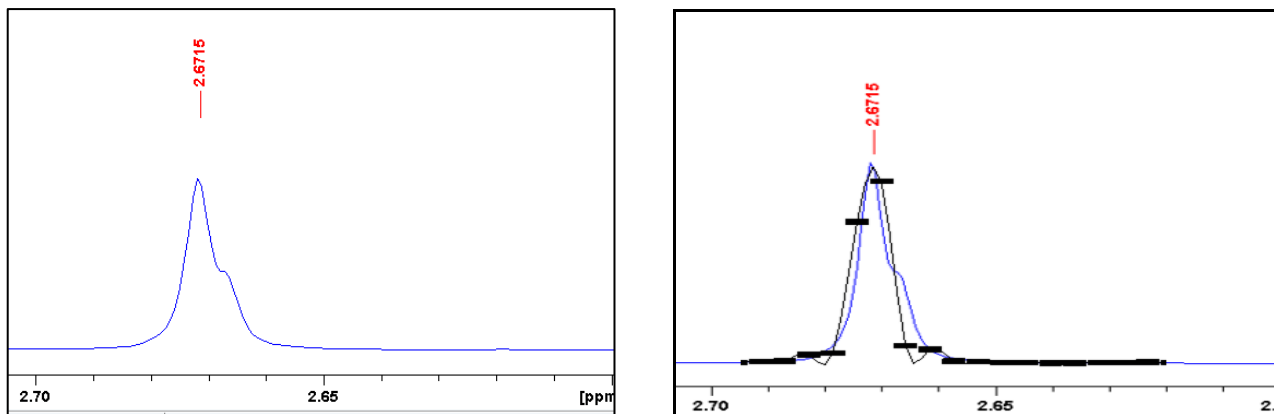


Figure S41. Time-dependent evolution of the abundance of **N-Me** according to the MCR-ALS analysis with one component of the ^1H NMR spectrum of HMTA and its decomposition products in the region $\delta_{\text{H}} = 2.60\text{-}2.70$ ppm.

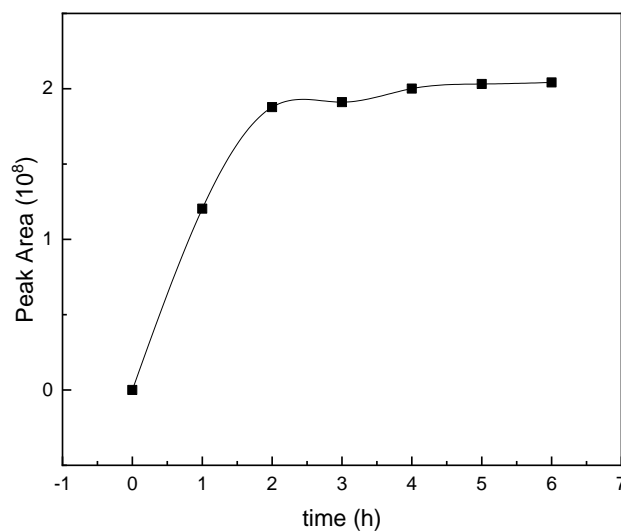


Figure S42. Left: ^1H NMR spectrum of HMTA and its decomposition products in the region $\delta_{\text{H}} = 4.50\text{-}4.77$ ppm. Right: Signal overlap with the “Pure” spectrum provided by MCR-ALS.

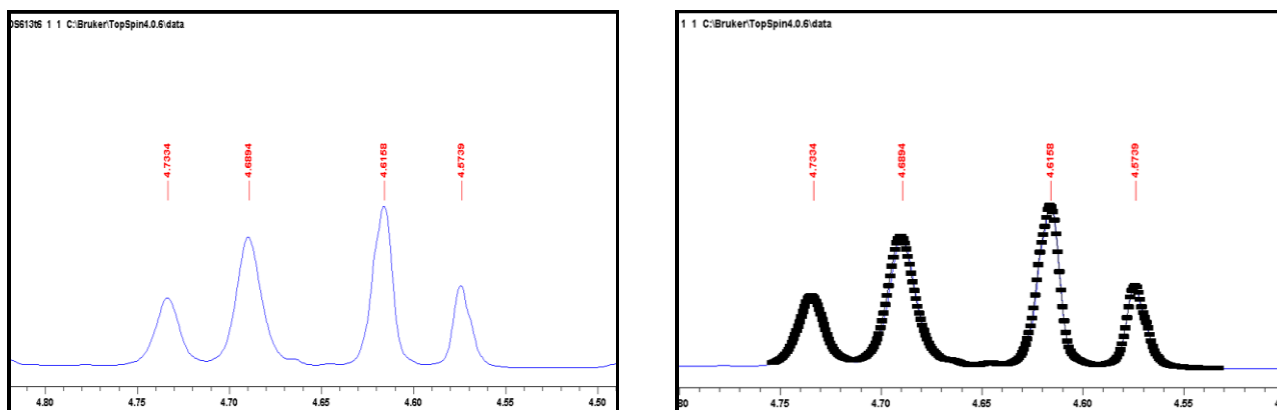


Figure S43. Time-dependent evolution of the abundance of **N-Me** according to the MCR-ALS analysis with one component of the ^1H NMR spectrum of HMTA and its decomposition products in the region $\delta_{\text{H}} = 4.50\text{-}4.77$ ppm.

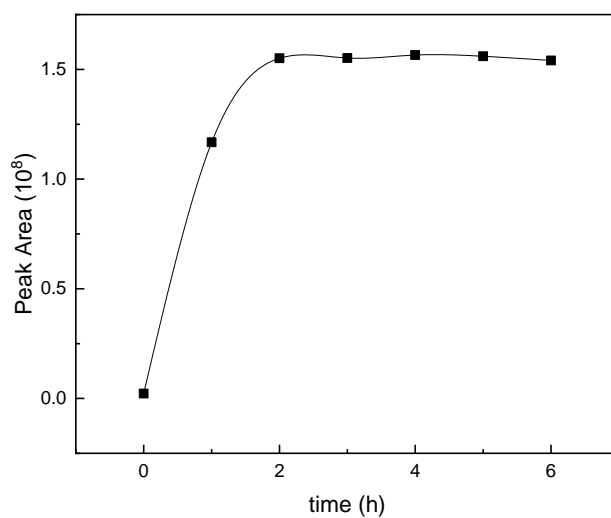


Figure S44. Left: ^1H NMR spectrum of HMTA and its decomposition products in the region $\delta_{\text{H}} = 4.90\text{--}5.01$ ppm. Right: Signal overlap with the “Pure” spectrum provided by MCR-ALS.

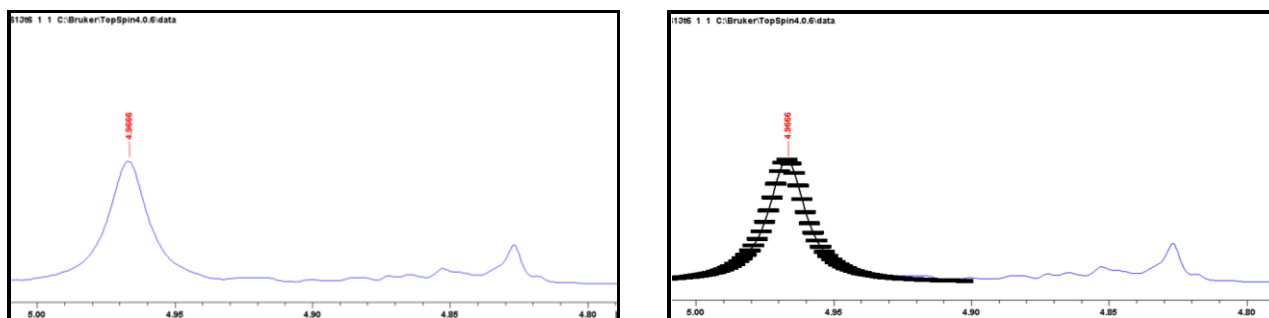


Figure S45. Time-dependent evolution of the abundance of **HMTA** according to the MCR-ALS analysis with one component of the ^1H NMR spectrum of HMTA and its decomposition products in the region $\delta_{\text{H}} = 4.90\text{--}5.08$ ppm.

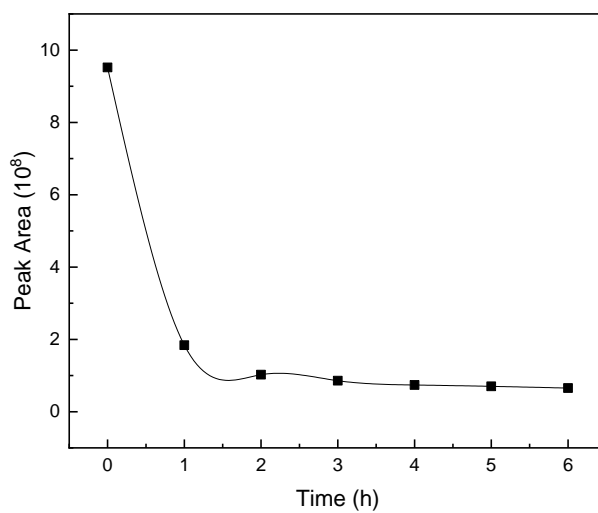


Figure S46. Left: ^1H NMR spectrum of HMTA and its decomposition products in the region $\delta_{\text{H}} = 5.10\text{-}5.16$ ppm. Right: Signal overlap with the “Pure” spectrum provided by MCR-ALS.

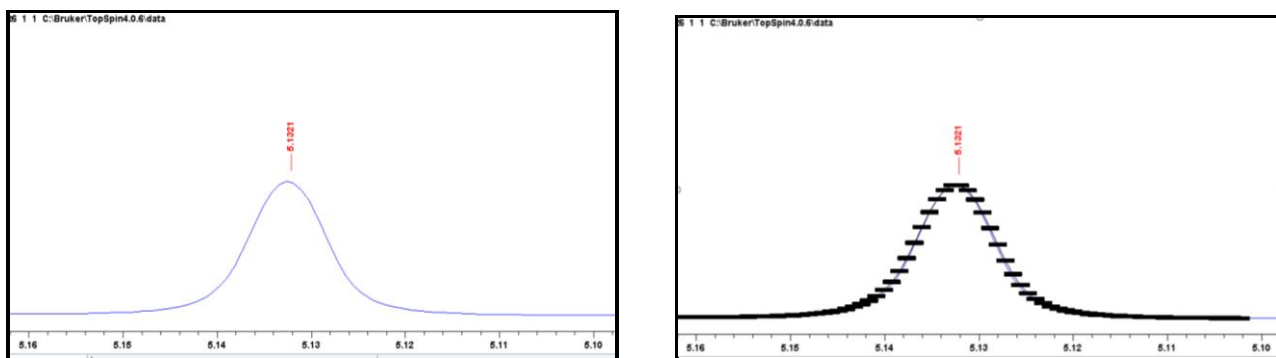


Figure S47. Time-dependent evolution of the abundance of N-Me according to the MCR-ALS analysis with one component of the ^1H NMR spectrum of HMTA and its decomposition products in the region $\delta_{\text{H}} = 5.10\text{-}5.16$ ppm.

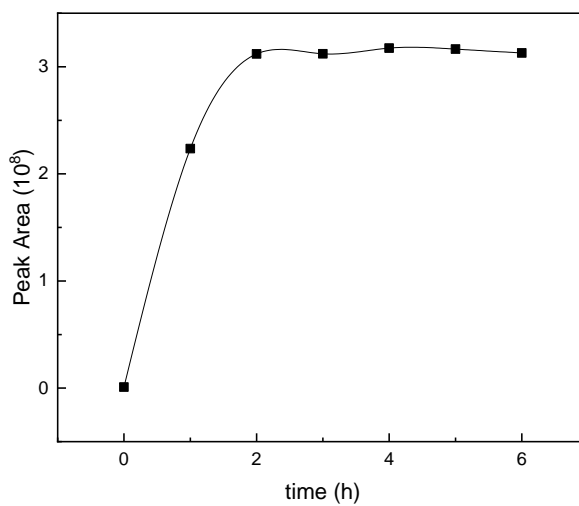
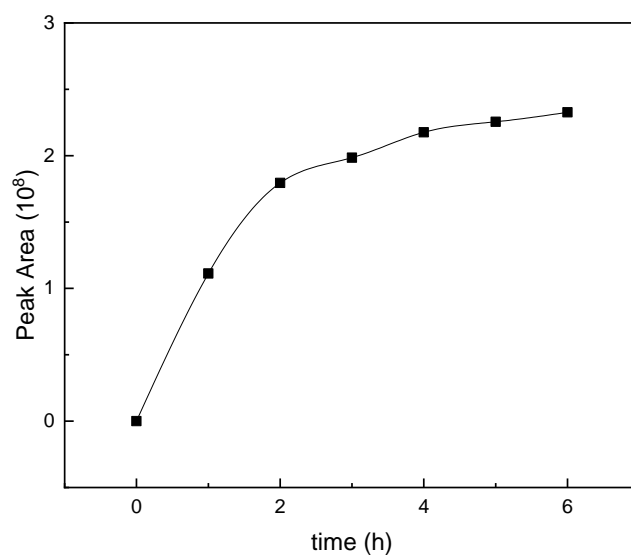


Figure S48. Time-dependent evolution of the abundance of **N-Me** according to the MCR-ALS analysis with one component of the ^1H NMR spectrum of HMTA and its decomposition products in the region $\delta_{\text{H}} = 8.00\text{-}8.50$ ppm.



Kinetic study of the decomposition of HMTA at 363 K

Experimental Procedure

Three solutions of HMTA in AcOH- d_4 were prepared at three different concentrations (0.36 M, 0.54 M and 0.72 M), and transferred to the corresponding NMR tubes. In the NMR spectrometer, the probe was set to 363 K. To carry out the experiment, the tubes were sequentially placed in the probe and ^1H NMR spectra were acquired every 3 minutes during 120 minutes.

The spectra were normalized considering the area under the residual methyl signal of AcOH- d_4 as the reference standard, and the concentrations (relative abundances) of the species were calculated using the MatLab routines. The concentrations of the species were plotted vs. time and their half-life times were calculated at the three concentrations.

To calculate reaction order and kinetic constant of HMTA at 363 K, the initial rates method was employed. At this end, spectra were acquired every 3 minutes, until the concentration of HMTA suffered a 20% reduction. The initial rates vs. time were plotted and the graph was fit with polynomials of different degrees. The first term of the polynomial that offered the best fit was taken as the initial rate for each concentration (In our case, the polynomial of third order gave the best fit, with $r^2 = 0.991$).

To calculate the kinetic constant, Concentration vs. time were plotted and the graph was fit with the equation: $C = (C_0 - C_f) \cdot e^{-kt} + C_f$. The fit of this equation gave a $r^2 = 0.999$.

The equation $\log V_0 = \log k + n \cdot \log C_0$ was applied to calculate the reaction constant and the reaction order. With both methods (half-life time and initial rates), the reaction afforded the following parameters.

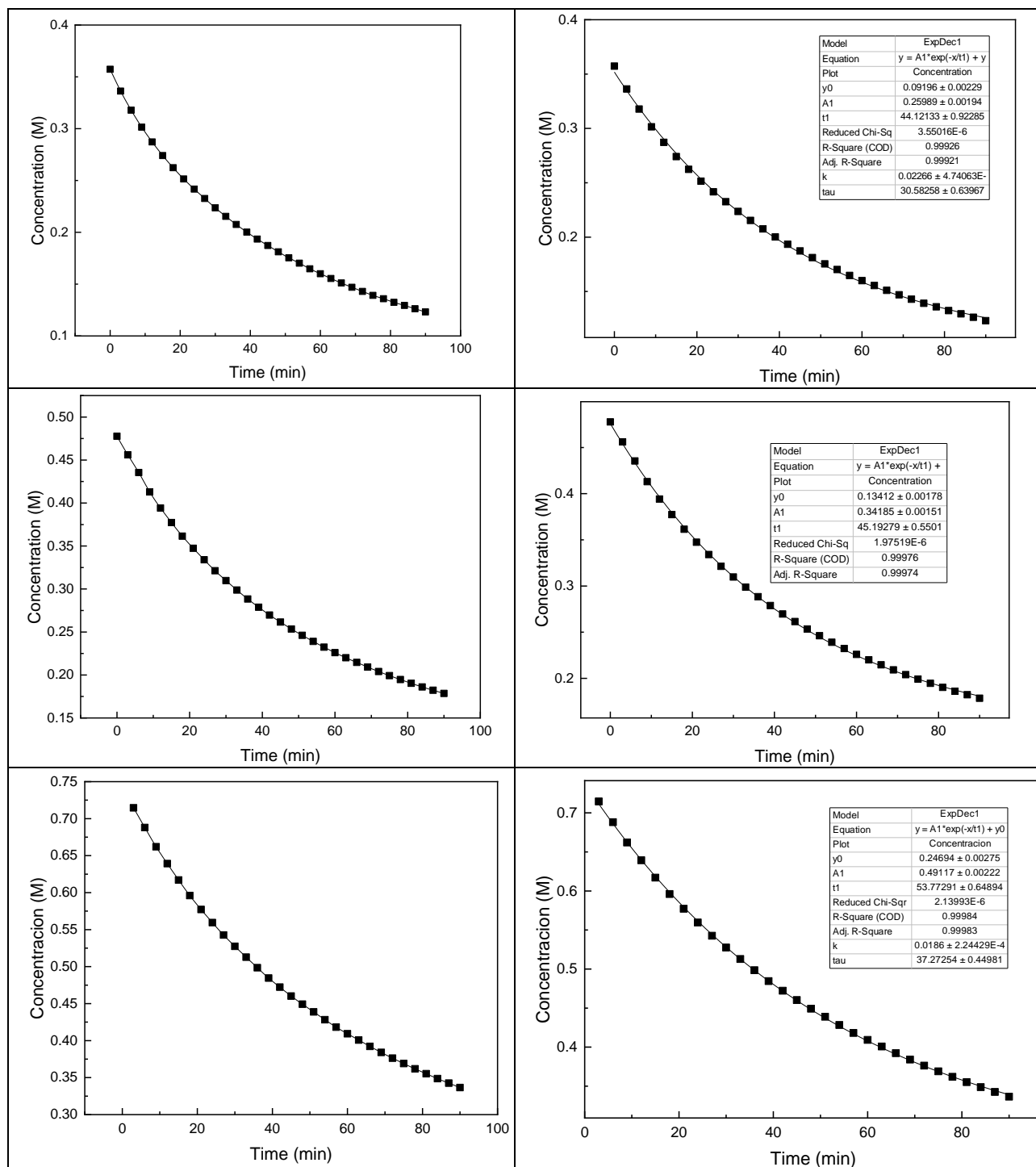
Reaction order: 1 (calculated value: 1.05)

Half-life time: 54 min

Kinetic constant at 363 K: 0.0186 min^{-1}

Decomposition rate of HMTA

Figure S49. Left: Time-dependent decomposition of HMTA at 363 K in AcOH- d_4 solutions of different concentrations [0.36 M (top), 0.54 M (middle) and 0.72 M (bottom)] in the 90 min experiment. Right: Exponential fits of the concentration vs. time plots (calculation of the kinetic constant).



Decomposition rate of HMTA

Figure S50. Polynomial fits of the decomposition rate vs. time for HTMA solutions of different concentrations (0.36 M, 0.54 M and 0.72 M).

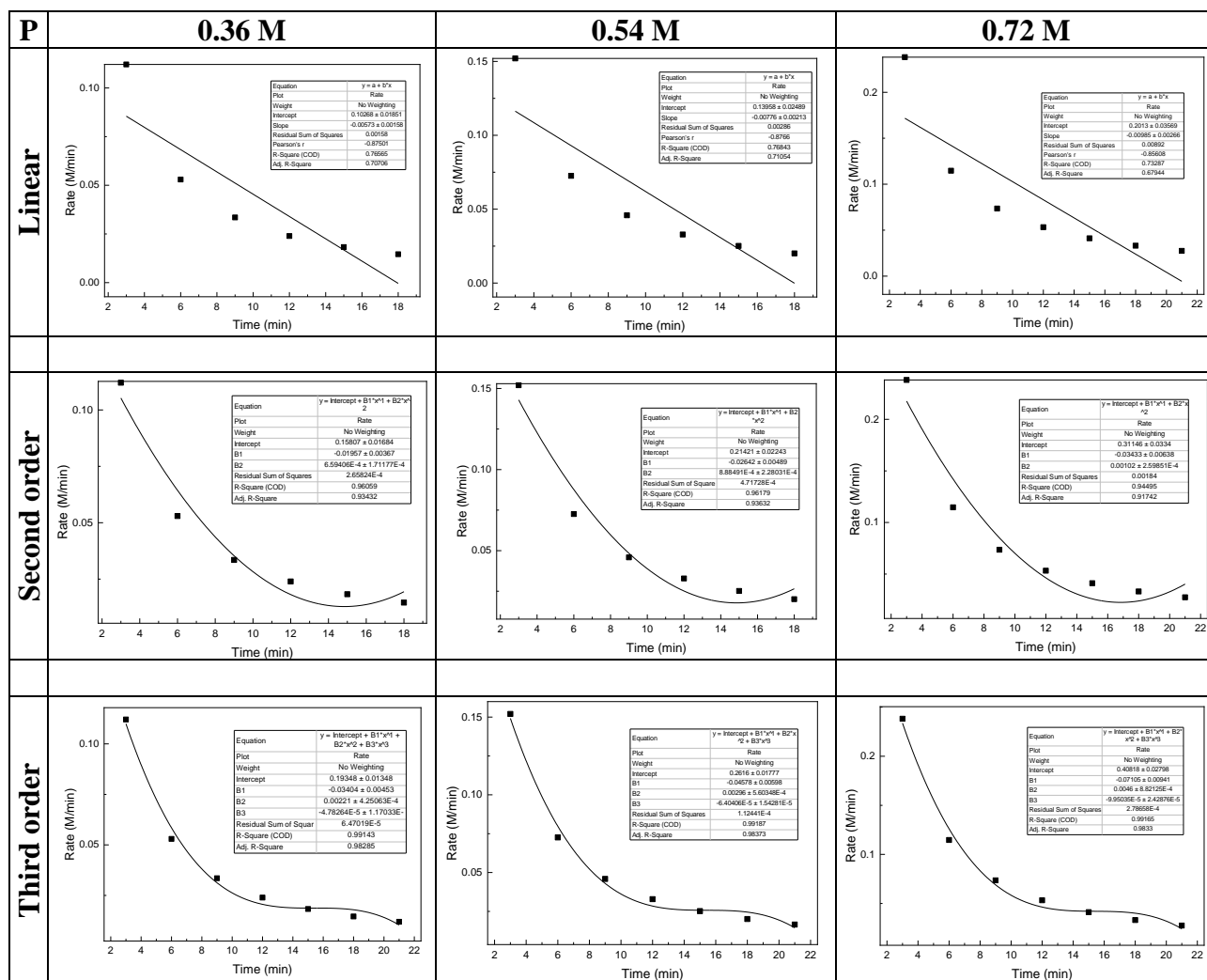
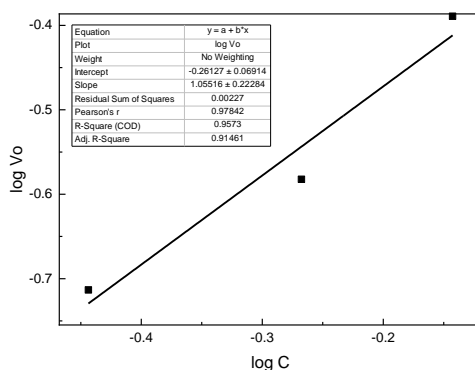


Figure S51. Calculation of reaction order by the initial rates method.



Reaction order: $n = 1.05 \pm 0.22$

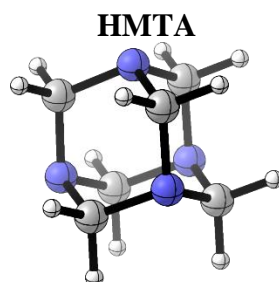
Computational methods

General information

Conformational searches for the reactants, transition structures (TS) and the products were run using the conformational search module of Hyperchem with the MM+ method.³ Selected structures were then successively optimized at the B3LYP/6-31G* and M062X/6-311+G** level of theory including the solvent (AcOH, $\epsilon = 6.15$) via the Solvation Model based on Density (SMD).⁴ This level has been shown as a perfect level of theory for this type of structures.⁵

Frequency calculations were made to confirm the nature of the stationary points and to evaluate their thermochemical properties. The molecular orbitals of the reactants were calculated to analyze the frontier orbital interactions at the M062X/6-311+G** level of theory. Intrinsic reaction coordinate (IRCs) calculations were run to verify the connectivity between reactants, TSs and products. To examine the more important interactions in the TSs, natural bond orbital calculations were performed and Wiberg bond indexes (WBIs) analyzed.

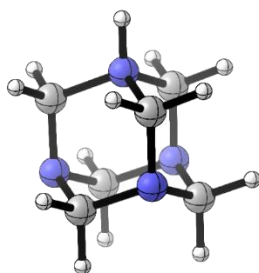
Cartesian Coordinates



(SMD-AcOH)-M062X/6-311+G** Free Energy = -454.625558

N	1.11363200	0.36616700	-0.93016300
C	1.63668400	-0.01800200	0.38903500
N	0.56772100	-0.38518200	1.33018900
C	-0.33887000	0.76605500	1.45872400
N	-0.91528500	1.17228700	0.16828800
C	0.19332300	1.49751000	-0.74139000
C	-0.19271500	-1.49770100	0.74155600
N	-0.76633500	-1.15378500	-0.56828200
C	0.33825700	-0.76594200	-1.45858600
C	-1.63644500	0.01834100	-0.38916000
H	2.20005600	0.82096100	0.80355100
H	2.30902400	-0.87013800	0.26765700
H	0.21650600	1.60785400	1.87811600
H	-1.15053600	0.50279700	2.14044800
H	0.75116300	2.34172800	-0.33019100
H	-0.21830600	1.78388500	-1.71174200
H	-1.00297600	-1.77076800	1.42108600
H	0.47239700	-2.35574300	0.62120900
H	-0.07288400	-0.48864000	-2.43171500
H	1.00490300	-1.62142200	-1.58725800
H	-2.45332300	-0.24692400	0.28563400
H	-2.05555600	0.29843400	-1.35810000

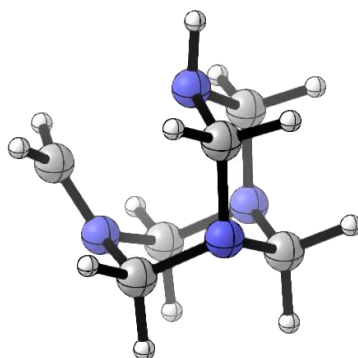
HMTAH⁺



(SMD-AcOH)-M062X/6-311+G** Free Energy = -455.055802

N	0.50927800	-1.18115900	-0.76477400
C	0.98576000	-1.23810100	0.62608400
N	0.51983900	-0.07686800	1.40191000
C	0.99410500	0.06472100	-1.38022100
N	0.52788500	1.24719500	-0.63807500
C	1.00362900	1.15161400	0.75136000
C	-0.91063800	1.28003400	-0.64885700
N	-1.44118900	0.01064100	0.00122600
C	-0.92953400	-1.19254100	-0.77738600
C	-0.91887600	-0.06796900	1.42849100
H	2.07525200	-1.24413300	0.62421700
H	0.62013300	-2.15281900	1.09443700
H	0.63419900	0.12049700	-2.40837700
H	2.08357600	0.05645000	-1.37802200
H	0.65025300	2.01801900	1.31198600
H	2.09306500	1.14266700	0.74903800
H	-1.29918200	1.30625700	-1.66686900
H	-1.29334000	2.12117800	-0.07093400
H	-2.46523000	0.01962400	0.00214300
H	-1.31842300	-1.10872900	-1.79209200
H	-1.32339500	-2.08336900	-0.28806600
H	-1.31377700	-0.98529600	1.86488500
H	-1.30049300	0.80444900	1.95882000

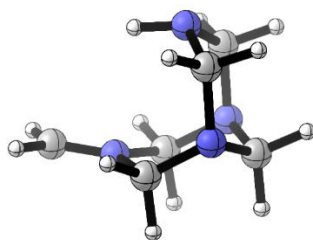
TSHMTA-H⁺



(SMD-AcOH)-M062X/6-311+G** Free Energy =-455.02052
Number of Imaginary Frequencies: 1 (-263.43)

N	-0.46528700	1.20477200	0.71143900
C	0.97948000	1.24239300	0.65144900
N	1.48136300	0.00000300	-0.01129000
C	-0.88643000	0.00001200	1.43210900
N	-0.46528300	-1.20476400	0.71146300
C	0.97948400	-1.24237500	0.65147200
C	-1.11471200	-1.21978200	-0.60405800
N	-0.80453500	-0.00001300	-1.37790600
C	-1.11471700	1.21976900	-0.60407900
C	1.58943300	-0.00001200	-1.29093900
H	1.38915800	1.26931400	1.66044700
H	1.32944900	2.09896300	0.07681000
H	-1.97307500	0.00001000	1.52261600
H	-0.44152300	0.00002700	2.42809200
H	1.32946100	-2.09895400	0.07685300
H	1.38916100	-1.26927600	1.66047000
H	-2.19288400	-1.31491900	-0.42767900
H	-0.77239900	-2.08949700	-1.16725200
H	-1.33482100	-0.00002500	-2.24488300
H	-2.19288900	1.31490600	-0.42770300
H	-0.77240500	2.08947300	-1.16729000
H	1.71186400	0.93873700	-1.82108700
H	1.71186300	-0.93877500	-1.82106200

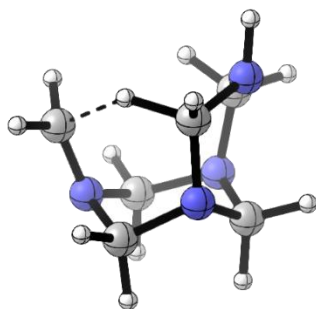
Iminium



(SMD-AcOH)-M062X/6-311+G** Free Energy = -455.031843

C	0.966427	-0.000551	1.375868
N	0.572623	1.201743	0.637265
N	0.571882	-1.202191	0.636554
C	-0.854189	-1.273580	0.551492
N	-1.463135	0.000257	0.010140
C	-0.853460	1.273486	0.551826
C	1.261178	1.208186	-0.667633
C	1.260367	-1.208320	-0.668327
N	1.085299	0.000205	-1.463342
C	-2.440254	0.000702	-0.795885
H	0.489302	-0.000724	2.357714
H	2.048683	-0.000826	1.503256
H	-1.279458	-1.390623	1.550543
H	-1.180785	-2.085422	-0.098100
H	-1.179683	2.085694	-0.097471
H	-1.278788	1.390491	1.550859
H	2.324935	1.328329	-0.449800
H	0.924767	2.071194	-1.241653
H	0.923158	-2.070729	-1.242796
H	2.323995	-1.329493	-0.450557
H	0.187880	0.000632	-1.933987
H	-2.856084	-0.943051	-1.137984
H	-2.855021	0.944894	-1.138386

[1,5]-H-Shift

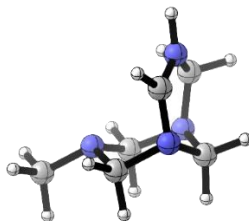


(SMD-AcOH)-M062X/6-311+G** Free Energy = -454.995075

Number of Imaginary Frequencies: 1 (-867.76)

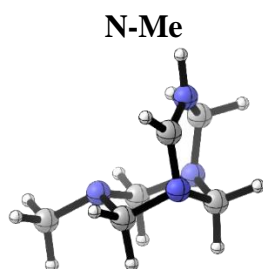
N	1.52663900	0.28796400	-0.36104900
C	1.49649700	-0.43775100	0.92134000
N	0.07801100	-0.73502700	1.14105800
C	-0.62399100	0.54520600	1.37466000
N	-0.69380900	1.27668800	0.11906900
C	0.66729300	1.50477300	-0.35984800
C	-1.59981500	0.55083500	-0.78110300
N	-1.73038900	-0.85452400	-0.35953600
C	-0.52659900	-1.44398700	0.04960200
C	1.41137000	-0.54900500	-1.38944100
H	1.86950200	0.18598900	1.72865200
H	2.08909700	-1.34714600	0.83573800
H	-0.06452200	1.11211200	2.11680000
H	-1.62580600	0.34909200	1.74897000
H	1.14382000	2.21988800	0.31037500
H	0.65228100	1.90603100	-1.37071000
H	-1.22911800	0.62676200	-1.80880100
H	-2.59311000	0.99893100	-0.73534200
H	-2.24835500	-1.41973800	-1.02186900
H	-0.57158100	-2.52412000	0.18373300
H	0.26025300	-1.37316500	-0.90698100
H	1.03683400	-0.16703400	-2.33416900
H	2.06901000	-1.41373800	-1.41445400

Imine-NMe



(SMD-AcOH)-M062X/6-311+G** Free Energy = -455.044033

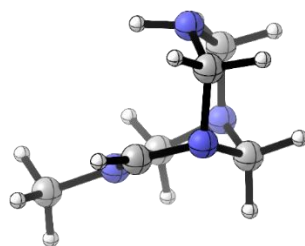
N	0.422750	1.191392	0.637421
C	1.044919	1.282470	-0.569251
N	1.760570	0.311096	-1.030220
C	1.642177	-1.082883	-0.491747
N	0.675205	-1.157941	0.568171
C	0.857548	0.012141	1.406189
C	-1.039584	1.141378	0.429434
C	-0.738913	-1.256620	0.198705
N	-1.302568	-0.032272	-0.401836
C	-2.736538	-0.200039	-0.606392
H	0.899282	2.177909	-1.167841
H	2.268589	0.447510	-1.900303
H	2.627388	-1.376486	-0.130033
H	1.352414	-1.712037	-1.332445
H	1.905320	0.127815	1.681126
H	0.246406	-0.048657	2.304440
H	-1.376606	2.039705	-0.091085
H	-1.510144	1.090990	1.419897
H	-1.278971	-1.510061	1.123452
H	-0.868595	-2.071487	-0.513600
H	-3.274724	-0.370194	0.338329
H	-3.144945	0.692770	-1.083821
H	-2.914771	-1.052385	-1.264489



(SMD-AcOH)-M062X/6-311+G** Free Energy = -454.612962

N	-1.27736300	-0.02827800	-0.39700400
C	-0.93182600	1.17230300	0.36472600
N	0.51253400	1.21746400	0.60848500
C	0.90492100	0.03116300	1.37401300
N	0.66288400	-1.16666500	0.58291000
C	-0.76077400	-1.22906600	0.27526500
C	1.54632200	-1.09364400	-0.58049000
N	1.75134800	0.22489000	-1.18360600
C	1.20353200	1.22605100	-0.63550300
C	-2.71843300	-0.12698900	-0.55973600
H	1.24035500	2.19663300	-1.12992200
H	-1.43597000	1.19293400	1.34373600
H	-1.23773500	2.05271200	-0.20589100
H	0.32179200	0.00197200	2.29547200
H	1.96501200	0.10076900	1.62092400
H	-1.28618400	-1.38491800	1.23312100
H	-0.95834300	-2.08989500	-0.36620100
H	1.15342800	-1.74726800	-1.36118400
H	2.53209500	-1.47357300	-0.29912700
H	-2.96407900	-1.00552000	-1.16081800
H	-3.24516100	-0.21172300	0.40510200
H	-3.09348200	0.75709300	-1.08035800

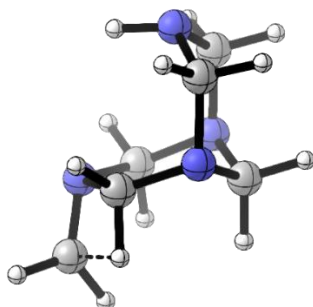
Iminium 2



(SMD-AcOH)-M062X/6-311+G** Free Energy = -455.050046

C	0.724156	0.318384	-1.415641
N	0.518624	-1.018708	-0.829379
N	0.475864	1.318369	-0.392673
C	-0.922961	1.271884	-0.078790
N	-1.460216	-0.127192	0.006482
C	1.583410	-1.268015	0.202829
C	1.430259	1.101870	0.717256
N	1.530687	-0.260574	1.238430
H	0.039007	0.450721	-2.252941
H	1.751055	0.376006	-1.772359
H	-1.507559	1.780204	-0.848218
H	-1.122469	1.728819	0.891757
H	2.534215	-1.224581	-0.327154
H	1.445584	-2.259672	0.630827
H	1.177046	1.772964	1.535663
H	2.407105	1.386215	0.320415
H	0.774630	-0.455267	1.888665
C	-2.833875	-0.263901	0.487417
H	-2.919595	0.222105	1.459468
H	-3.507010	0.218970	-0.222460
H	-3.083959	-1.319952	0.570733
C	-0.712769	-1.147195	-0.258332
H	-1.052083	-2.137962	0.037153

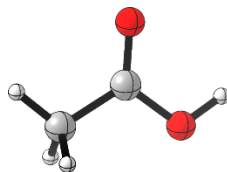
[1,3]-H-Shift



(SMD-AcOH)-M062X/6-311+G** Free Energy = -454.940472
Number of Imaginary Frequencies: 1 (-431.3956)

C	-0.296986	0.104641	1.452349
N	-0.116363	-1.144439	0.696673
N	-0.523083	1.220460	0.547573
C	0.671615	1.488839	-0.198809
N	1.371241	0.280536	-0.810330
C	-1.328560	-1.383234	-0.138084
C	-1.716940	0.969453	-0.272688
N	-1.697320	-0.287671	-1.006286
H	0.585644	0.295252	2.068248
H	-1.159949	-0.022953	2.104787
H	1.398855	1.984551	0.449002
H	0.441957	2.138270	-1.041394
H	-2.135926	-1.559215	0.575723
H	-1.174246	-2.289456	-0.722010
H	-1.844176	1.796411	-0.969853
H	-2.568204	0.952130	0.412176
H	-1.076986	-0.229362	-1.808774
C	2.504852	-0.081840	-0.165724
H	3.234798	-0.695392	-0.689782
H	2.812333	0.406976	0.761705
H	1.917318	-1.381075	0.558442
C	1.042812	-1.101636	-0.139102
H	1.066498	-1.855684	-0.919333

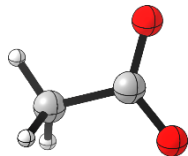
Acetic Acid



(SMD-AcOH)-M062X/6-311+G** Free Energy = -229.031700

O	-0.85330600	-0.99897200	0.00000100
C	-0.12128900	0.12998500	-0.00000100
O	-0.69322900	1.19093500	-0.00001600
C	1.36723100	-0.04146800	0.00001100
H	-0.29241600	-1.78646200	0.00002100
H	1.84821900	0.93342900	0.00003300
H	1.67040600	-0.60690000	0.88444800
H	1.67041900	-0.60687300	-0.88443900

Acetate



(SMD-AcOH)-M062X/6-311+G** Free Energy = -228.571855

C	0.08620900	0.11984200	0.00005400
O	0.62081500	1.20315000	-0.00002100
O	0.79125700	-1.02154800	-0.00001300
H	1.73771100	-0.80883800	-0.00002200
C	-1.38682000	-0.12679800	-0.00000600
H	-1.65515500	-0.71167800	-0.88196600
H	-1.65528400	-0.71097500	0.88238500
H	-1.92018500	0.82041600	-0.00040400

References

- 1 N. L. Calvo, N. M. Balzaretti, M. Antonio, T. S. Kaufman and R. M. Maggio, *J. Pharm. Biomed. Anal.*, 2018, **158**, 461–470.
- 2 J. Jaumot, R. Gargallo, A. de Juan and R. Tauler, *Chemom. Intell. Lab. Syst.*, 2005, **76**, 101–110.
- 3 Hyperchem Professional Release 7.52, Hypercube, Inc., 2005.
- 4 Gaussian 09, Revision D.01: M. J. Frisch, G. W. Trucks, H. B. Schlegel, G. E. Scuseria, M. A. Robb, J. R. Cheeseman, G. Scalmani, V. Barone, B. Mennucci, G. A. Petersson, H. Nakatsuji, M. Caricato, X. Li, H. P. Hratchian, A. F. Izmaylov, J. Bloino, G. Zheng, J. L. Sonnenberg, M. Hada, M. Ehara, K. Toyota, R. Fukuda, J. Hasegawa, M. Ishida, T. Nakajima, Y. Honda, O. Kitao, H. Nakai, T. Vreven, J. A. Montgomery, Jr., J. E. Peralta, F. Ogliaro, M. Bearpark, J. J. Heyd, E. Brothers, K. N. Kudin, V. N. Staroverov, T. Keith, R. Kobayashi, J. Normand, K. Raghavachari, A. Rendell, J. C. Burant, S. S. Iyengar, J. Tomasi, M. Cossi, N. Rega, J. M. Millam, M. Klene, J. E. Knox, J. B. Cross, V. Bakken, C. Adamo, J. Jaramillo, R. Gomperts, R. E. Stratmann, O. Yazyev, A. J. Austin, R. Cammi, C. Pomelli, J. W. Ochterski, R. L. Martin, K. Morokuma, V. G. Zakrzewski, G. A. Voth, P. Salvador, J. J. Dannenberg, S. Dapprich, A. D. Daniels, O. Farkas, J. B. Foresman, J. V. Ortiz, J. Cioslowski, and D. J. Fox, Gaussian, Inc., Wallingford CT, 2013.
- 5 A. V. Marenich, C. J. Cramer, D. G. Truhlar, *J. of Phys. Chem. B* **2009**, *113*, 6378-6396; N. Grimblat, A. M. Sarotti, T. S. Kaufman and S. O. Simonetti, *Org. Biomol. Chem.*, 2016, **14**, 10496–10501.